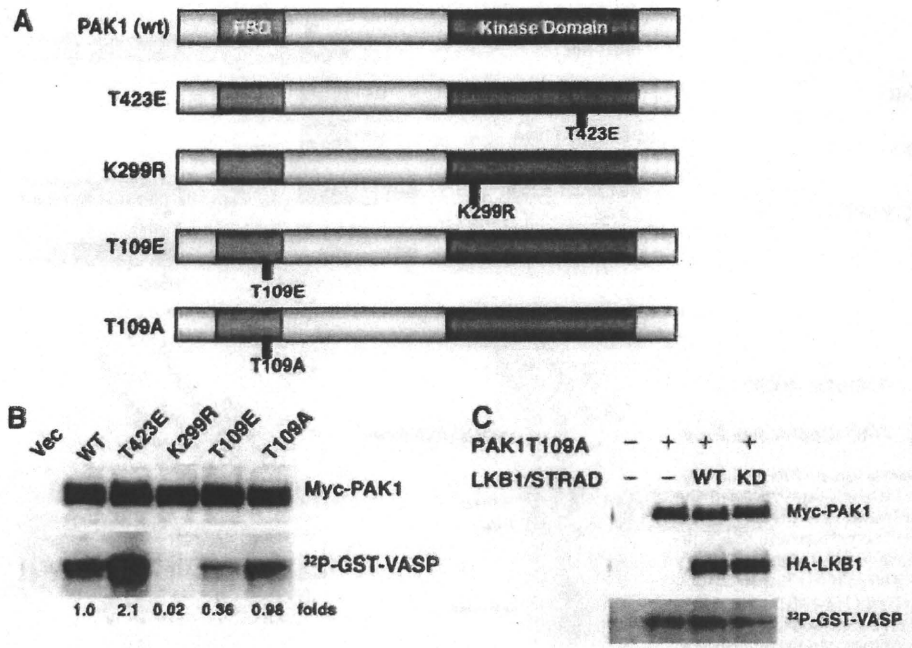

FIGURE 5. **Phosphorylation of PAK1 at Thr^{109} reduces its activity.** *A*, structures of PAK1 constructs. wt PAK1 contains the p21-binding domain (*light gray*) and the kinase domain (*dark gray*). The noncatalytic domains are in *white*. Also displayed are the constitutively active mutant (T423E), dominant-negative mutant (K299R), phosphorylation-mimicked mutant for Thr^{109} (T109E), and the nonphosphorylatable mutant for Thr^{109} (T109A). *B*, the kinase activities of PAK1 mutants. The HEK293T cells were co-transfected with the indicated constructs. At 24 h post-transfection, the immunoprecipitates were prepared with an anti-Myc antibody. The precipitates were used for *in vitro* kinase assays using GST-VASP-(158–277) as a substrate. Cellular levels of Myc-PAK1 were determined by Western blotting with anti-Myc antibody. *C*, LKB1 (wt or kinase-dead (*KD*)) failed to inhibit the activity of the PAK1-T109A mutant. Cultured HEK293T cells were co-transfected with the indicated constructs. The kinase activities were determined as described under "Experimental Procedures." Cellular levels of Myc-PAK1 and HA-LKB1 were determined by Western blotting with anti-Myc or anti-HA antibody. Similar results were obtained in three independent experiments. *Vec*, vector.

strate for LKB1 and that Thr^{109} is a likely target of phosphorylation by LKB1, although it is possible that LKB1 phosphorylates other residues of PAK1 in addition to Thr^{109}. To determine whether LKB1 phosphorylates PAK1 at Thr^{109} *in vivo*, we performed a series of mass spectrometric analyses of PAK1 purified from HEK293T cells transiently co-transfected with plasmids encoding PAK1 and LKB1/STRAD (supplemental Fig. S1). The protonated molecular ions of peptide LLQTSNITK-(106–114) obtained from tryptic digestion of wt-PAK1 were detected in its nonphosphorylated form ($[M + H]^+$ at m/z 1017.55) and in its monophosphorylated form ($[M + H]^+$ at m/z 1097.54). To further confirm the specific phosphorylation site of the peptide, we used HEK293T cells co-transfected with plasmids encoding PAK1-T109A and LKB1/STRAD for another set of mass spectrometric analyses. The molecular ion of LLQASNITK appeared at m/z 987.59 corresponding to the substitution of threonine at residue 109 with alanine. Notably, the corresponding monophosphopeptide was not detected in PAK1-T109A, excluding phosphorylation at the other Thr or Ser residue of the peptide. These results are consistent with our interpretation that LKB1 phosphorylates PAK1 at Thr^{109} *in vivo*.

Phosphorylation of PAK1 at Thr^{109} by LKB1 Reduces Its Activity—We have demonstrated that the kinase activity of LKB1 is necessary to inhibit that of PAK1 (Fig. 3*A*). Therefore, we next investigated whether phosphorylation of Thr^{109} by LKB1 regulated PAK1 activity. Namely, we constructed a PAK1-T109E mutant whose amino acid residue 109 was converted to glutamic acid from threonine. This substitution mimics the phosphorylation of threonine with the acidic moiety of glutamic acid. As an inactive (negative) control, we also constructed the alanine substitution PAK1-T109A (Fig. 5*A*). We transiently transfected HEK293T cells with plasmids encoding these constructs of PAK1: wt, constitutively-active (T423E), dominant-negative (K299R), T109E, and T109A, respectively (Fig. 5*A*). We then determined the *in vitro* PAK1 activities in the cell lysates using GST-VASP-(158–277) as substrate. The PAK1 mutant T423E showed the highest activity (2.1×), whereas mutant K299R with defective kinase (kinase-dead) had only 2% of the wt-PAK1 activity. Notably, T109E mutant showed significantly reduced PAK1 activity (36% of wt), whereas T109A mutant had a similar activity to the wt (98%) (Fig. 5*B*). These results suggest that phosphorylation of PAK1 at Thr^{109} decreases its kinase activity. To confirm the role of phosphorylation at Thr^{109} in suppression of PAK1 activity by LKB1, we next tested nonphosphorylatable PAK1-T109A in HEK293T cells. Co-expression of LKB1 failed to suppress the activity of PAK1-T109A (Fig. 5*C*), in sharp contrast to the effect on wt-PAK1 (Fig. 3*A*). These results strongly suggest that LKB1 suppresses the PAK1 activity by phosphorylating it at Thr^{109}.

Activation of PAK1 in Lkb1(+/−) Mouse HCCs and Lkb1(−/−) MEFs—We have previously demonstrated that *Lkb1*(+/−) mice develop HCC after 50 weeks of age and that HCCs and nodular foci of *Lkb1*(+/−) liver show loss of the *Lkb1* heterozygosity (10, 11). To test the involvement of LKB1 in PAK1-mediated signaling *in vivo*, we next determined the level of phosphorylated form of PAK1 in HCCs of *Lkb1*(+/−) mice, using two different types of phospho-specific PAK1 antibodies that recognized the active form of PAK1. Notably, we found that the level of phosphorylated PAK1 was increased in HCCs (H1 and H2) and in precancerous lesions (nodular foci, F1 and F2), compared with the normal liver of *Lkb1*(+/−) or *Lkb1*(+/+) mice, while the levels of total PAK1 in nodular foci and HCCs were similar to those in normal liver (Fig. 6*A*). These results are therefore consistent with the interpretation that loss of LKB1 induces PAK1 activation. We further investigated the status of PAK1 activation in *Lkb1*(−/−) MEFs (MEF3-2) and wt MEFs. Both the level of phosphorylated PAK1 and *in vitro* PAK1 activity were significantly higher in *Lkb1*(−/−) MEFs

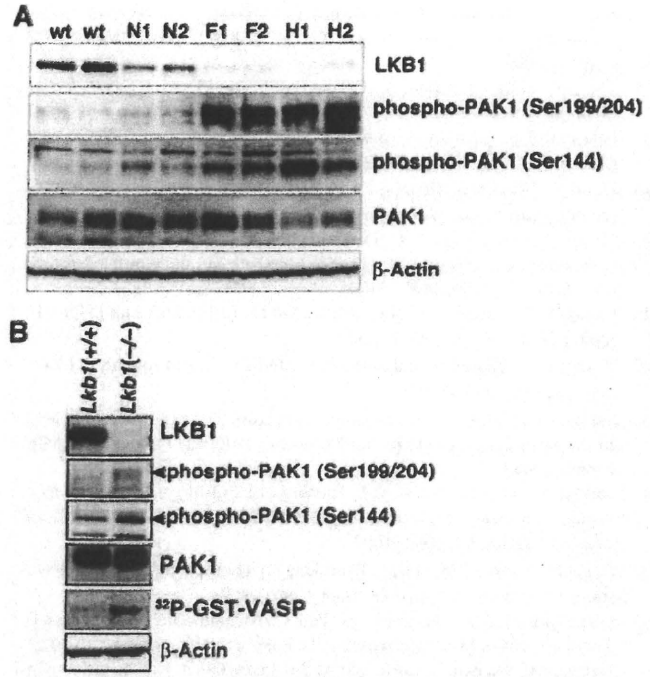

FIGURE 6. **Activation of PAK1 in *Lkb1*(+/−) mouse HCCs and *Lkb1*(−/−) MEFs.** *A*, activation of PAK1 in *Lkb1*(+/−) mice HCCs. Cellular levels of phospho-PAK1, PAK1, and β-actin in tissue lysates were determined by Western blotting with anti-phospho-PAK1 (Ser^{144}), anti-phospho-PAK1 ($Ser^{199/204}$), anti-PAK1, and anti-β-actin. Two wild-type livers (W1 and W2), pairs of tumor (H1 and H2), precancerous lesions (F1 and F2) and adjacent normal tissue (N1 and N2) from two *Lkb1*(+/−) mice were analyzed. *B*, increased PAK1 activity in *Lkb1*(−/−) MEFs. Cellular levels of phospho-PAK1, PAK1, and β-actin in tissue lysates were determined by Western blotting with the indicated antibodies. For *in vitro* kinase assay, cell lysates were prepared from MEF cells and immunoprecipitated using an anti-PAK1 antibody. The precipitates were used for *in vitro* kinase assays using GST-VASP-(158–277) as a substrate. The phosphorylation of GST-VASP was visualized using BAS-5000 Bio-imaging Analyzer. Similar results were obtained in three independent experiments.

than those in wt MEFs (Fig. 6*B*). These data together suggest that loss of LKB1 contributes to the activation of PAK1.

DISCUSSION

In this study, we have provided evidence that LKB1 inhibits PAK1 activation by direct phosphorylation of PAK1 at Thr^{109}. We first showed that knockdown of LKB1 increased cell migration and PAK1 activity in HCT116 cells (Fig. 1), whereas introduction of LKB1 in *Lkb1*-null MEFs reduced cell migration and PAK1 activity simultaneously (Fig. 2). Notably, a constitutively active mutant of PAK1 (PAK1-T423E) recovered the LKB1-mediated reduction of cell migration in a dose-dependent manner (Fig. 2*C*). Because HCCs in *Lkb1*(+/−) mice can metastasize to the lung (10), it is conceivable that inhibition of PAK1 by LKB1 contributes to suppression of cancer metastasis. We also demonstrated that LKB1 directly phosphorylated PAK1 at Thr^{109} both *in vitro* (Fig. 4) and *in vivo* (supplemental Fig. S1). Importantly, the phosphomimetic PAK1-T109E mutation reduced its activity (Fig. 5*B*), whereas the activity of a nonphosphorylatable mutant PAK1-T109A was not suppressed by LKB1 (Fig. 5*C*). These results indicate that phosphorylation of Thr^{109} is both necessary and sufficient for inhibition of PAK1 activity by LKB1, although it is possible that LKB1 phosphorylates other residues of PAK1 in addition to Thr^{109} (Fig. 4*C*). Consistently, we found that active forms of PAK1 were increased in the nodular foci and HCCs in *Lkb1*(+/−) mice, compared with the normal liver of *Lkb1*(+/−) and *Lkb1*(+/+) mice (Fig. 6*A*).

Our present results indicate that PAK1 is a novel LKB1 substrate. So far, 14 kinases have been identified as LKB1 substrates, including AMPKα1, AMPKα2, MARK1, and MARK2. LKB1 phosphorylates these kinases at the L*X*T motif in the activation loop (5, 37), and such phosphorylations can induce kinase activation. In contrast, LKB1-induced phosphorylation of PAK1 at Thr^{109} in the L*X*T motif of PBD causes a decrease in the kinase activity (Fig. 5*B*). Because this motif is well conserved among group I PAKs (PAK1, PAK2, and PAK3), it is likely that regulation of the PAK1 activity by LKB1 applies to PAK2 and PAK3 as well. According to the structural analysis of PAK1, Thr^{109} is located at the helix loop Iα in an inhibitory switch (38) and exposed to the outer space. In addition, the L107F mutation of PAK1 prevents the interaction between the autoinhibitory region and the C-terminal catalytic region, making the constitutively active kinase (39). Because this mutant lacks the L*X*T motif, the constitutive activation is likely due to the loss of negative regulation by LKB1. We therefore speculate that the phosphorylation of this Thr residue enhances the interaction between the autoinhibitory (N-terminal regulatory) and kinase domains, leading to inhibition of the PAK1 activity. Further experiments are required to elucidate the precise role of Thr^{109} phosphorylation in PAK1 conformation.

It has been reported recently that LKB1 maintains cancer cell polarity by recruiting Cdc42 to the leading edges and that inhibition of LKB1 reduces PAK1 autophosphorylation (40). In contrast, we have found that LKB1 suppresses PAK1 activity by direct phosphorylation. The reason for the discrepancy is not clear but may be related to the methods used to overexpress LKB1 (transient transfection of LKB1 expression vector alone *versus* co-infection of LKB1 with STRAD using adenovirus vector) or the cell context, genetic constitution such as p53 mutation status (non-small cell lung cancer cells (p53 mutant) *versus* HEK293T or *Lkb1*-null MEFs (wt-p53)). Notably, LKB1 plays key roles in growth arrest or apoptosis through a p53-dependent mechanism (41, 42). Thus, it is conceivable that LKB1-mediated PAK1 inhibition may be dependent on the p53 status.

Numerous PAK1 substrates and/or interacting proteins have been identified that activate diverse signaling processes involved in cell motility, morphology, growth, survival, and epithelial-mesenchymal transition (19). For example, PAK1 stabilizes microtubules through stathmin/Op18 phosphorylation (43, 44). Therefore, LKB1 also may contribute to microtubule destabilization by regulating PAK1, whereas we have reported previously that LKB1 inhibits tubulin polymerization through activation of MARK2 (17). Further investigation is needed to address the role of LKB1 in various downstream processes of PAK1 other than cell motility. In conclusion, our present results suggest that PAK1 is a novel downstream target of LKB1, and that LKB1-mediated PAK1 phosphorylation may play important roles in tumor suppression in the liver.

Acknowledgment—We thank Dr. J. Chernoff for PAK1 wild-type, T423E, H83LH86LK299R, and 86L-K299R constructs.

REFERENCES

1. Giardiello, F. M., Welsh, S. B., Hamilton, S. R., Offerhaus, G. J., Gittelsohn, A. M., Booker, S. V., Krush, A. J., Yardley, J. H., and Luk, G. D. (1987) *N. Engl. J. Med.* **316,** 1511–1514
2. Hemminki, A., Markie, D., Tomlinson, I., Avizienyte, E., Roth, S., Loukola, A., Bignell, G., Warren, W., Aminoff, M., Höglund, P., Järvinen, H., Kristo, P., Pelin, K., Ridanpää, M., Salovaara, R., Toro, T., Bodmer, W., Olschwang, S., Olsen, A. S., Stratton, M. R., de la Chapelle, A., and Aaltonen, L. A. (1998) *Nature* **391,** 184–187
3. Jenne, D. E., Reimann, H., Nezu, J., Friedel, W., Loff, S., Jeschke, R., Müller, O., Back, W., and Zimmer, M. (1998) *Nat. Genet.* **18,** 38–43
4. Launonen, V. (2005) *Hum. Mutat.* **26,** 291–297
5. Alessi, D. R., Sakamoto, K., and Bayascas, J. R. (2006) *Annu. Rev. Biochem.* **75,** 137–163
6. Katajisto, P., Vallenius, T., Vaahtomeri, K., Ekman, N., Udd, L., Tiainen, M., and Mäkelä, T. P. (2007) *Biochim. Biophys. Acta* **1775,** 63–75
7. Miyoshi, H., Nakau, M., Ishikawa, T. O., Seldin, M. F., Oshima, M., and Taketo, M. M. (2002) *Cancer Res.* **62,** 2261–2266
8. Rossi, D. J., Ylikorkala, A., Korsisaari, N., Salovaara, R., Luukko, K., Launonen, V., Henkemeyer, M., Ristimaki, A., Aaltonen, L. A., and Makela, T. P. (2002) *Proc. Natl. Acad. Sci. U.S.A.* **99,** 12327–12332
9. Bardeesy, N., Sinha, M., Hezel, A. F., Signoretti, S., Hathaway, N. A., Sharpless, N. E., Loda, M., Carrasco, D. R., and DePinho, R. A. (2002) *Nature* **419,** 162–167
10. Nakau, M., Miyoshi, H., Seldin, M. F., Imamura, M., Oshima, M., and Taketo, M. M. (2002) *Cancer Res.* **62,** 4549–4553
11. Miyoshi, H., Deguchi, A., Nakau, M., Kojima, Y., Mori, A., Oshima, M., Aoki, M., and Taketo, M. M., (2009) *Cancer Sci.* **100,** 2046–2053
12. Baas, A. F., Boudeau, J., Sapkota, G. P., Smit, L., Medema, R., Morrice, N. A., Alessi, D. R., and Clevers, H. C. (2003) *EMBO J.* **22,** 3062–3072
13. Boudeau, J., Baas, A. F., Deak, M., Morrice, N. A., Kieloch, A., Schutkowski, M., Prescott, A. R., Clevers, H. C., and Alessi, D. R. (2003) *EMBO J.* **22,** 5102–5114
14. Baas, A. F., Smit, L., and Clevers, H. (2004) *Trends. Cell Biol.* **14,** 312–319
15. Zhang, L., Li, J., Young, L. H., and Caplan, M. J. (2006) *Proc. Natl. Acad. Sci. U.S.A.* **103,** 17272–17277
16. Zheng, B., and Cantley, L. C. (2007) *Proc. Natl. Acad. Sci. U.S.A.* **104,** 819–822
17. Kojima, Y., Miyoshi, H., Clevers, H. C., Oshima, M., Aoki, M., and Taketo, M. M. (2007) *J. Biol. Chem.* **282,** 23532–23540
18. Partin, A. W., Isaacs, J. T., Treiger, B., and Coffey, D. S. (1988) *Cancer Res.* **48,** 6050–6053
19. Bokoch, G. M. (2003) *Annu. Rev. Biochem.* **72,** 743–781
20. Kumar, R., Gururaj, A. E., and Barnes, C. J. (2006) *Nat. Rev. Cancer* **6,** 459–471
21. Manser, E., Leung, T., Salihuddin, H., Zhao, Z. S., and Lim, L. (1994) *Nature* **367,** 40–46
22. Tsakiridis, T., Taha, C., Grinstein, S., and Klip, A. (1996) *J. Biol. Chem.* **271,** 19664–19667
23. King, C. C., Gardiner, E. M., Zenke, F. T., Bohl, B. P., Newton, A. C., Hemmings, B. A., and Bokoch, G. M. (2000) *J. Biol. Chem.* **275,** 41201–41209
24. Tang, Y., Zhou, H., Chen, A., Pittman, R. N., and Field, J. (2000) *J. Biol. Chem.* **275,** 9106–9109
25. Balasenthil, S., Sahin, A. A., Barnes, C. J., Wang, R. A., Pestell, R. G., Vadlamudi, R. K., and Kumar, R. (2004) *J. Biol. Chem.* **279,** 1422–1428
26. Holm, C., Rayala, S., Jirström, K., Stål, O., Kumar, R., and Landberg, G. (2006) *J. Natl. Cancer Inst.* **98,** 671–680
27. Carter, J. H., Douglass, L. E., Deddens, J. A., Colligan, B. M., Bhatt, T. R., Pemberton, J. O., Konicek, S., Hom, J., Marshall, M., and Graff, J. R. (2004) *Clin. Cancer Res.* **10,** 3448–3456
28. Ching, Y. P., Leong, V. Y., Lee, M. F., Xu, H. T., Jin, D. Y., and Ng, I. O. (2007) *Cancer Res.* **67,** 3601–3608
29. Wang, R. A., Zhang, H., Balasenthil, S., Medina, D., and Kumar, R. (2006) *Oncogene* **25,** 2931–2936
30. Sapkota, G. P., Kieloch, A., Lizcano, J. M., Lain, S., Arthur, J. S., Williams, M. R., Morrice, N., Deak, M., and Alessi, D. R. (2001) *J. Biol. Chem.* **276,** 19469–19482
31. Sandig, V., Youil, R., Bett, A. J., Franlin, L. L., Oshima, M., Maione, D., Wang, F., Metzker, M. L., Savino, R., and Caskey, C. T. (2000) *Proc. Natl. Acad. Sci. U.S.A.* **97,** 1002–1007
32. Deguchi, A., Soh, J. W., Li, H., Pamukcu, R., Thompson, W. J., and Weinstein, I. B. (2002) *Mol. Cancer. Ther.* **1,** 803–809
33. Ji, H., Ramsey, M. R., Hayes, D. N., Fan, C., McNamara, K., Kozlowski, P., Torrice, C., Wu, M. C., Shimamura, T., Perera, S. A., Liang, M. C., Cai, D., Naumov, G. N., Bao, L., Contreras, C. M., Li, D., Chen, L., Krishnamurthy, J., Koivunen, J., Chirieac, L. R., Padera, R. F., Bronson, R. T., Lindeman, N. I., Christiani, D. C., Lin, X., Shapiro, G. I., Jänne, P. A., Johnson, B. E., Meyerson, M., Kwiatkowski, D. J., Castrillon, D. H., Bardeesy, N., Sharpless, N. E., and Wong, K. K. (2007) *Nature* **448,** 807–810
34. Kumar, R., and Vadlamudi, R. K. (2002) *J. Cell. Physiol.* **193,** 133–144
35. Chong, C., Tan, L., Lim, L., and Manser, E. (2001) *J. Biol. Chem.* **276,** 17347–17353
36. Butt, E., Abel, K., Krieger, M., Palm, D., Hoppe, V., Hoppe, J., and Walter, U. (1994) *J. Biol. Chem.* **269,** 14509–14517
37. Lizcano, J. M., Göransson, O., Toth, R., Deak, M., Morrice, N. A., Boudeau, J., Hawley, S. A., Udd, L., Mäkelä, T. P., Hardie, D. G., and Alessi, D. R. (2004) *EMBO J.* **23,** 833–843
38. Lei, M., Lu, W., Meng, W., Parrini, M. C., Eck, M. J., Mayer, B. J., and Harrison, S. C. (2000) *Cell* **102,** 387–397
39. Brown, J. L., Stowers, L., Baer, M., Trejo, J., Coughlin, S., and Chant, J. (1996) *Curr. Biol.* **6,** 598–605
40. Zhang, S., Schafer-Hales, K., Khuri, F. R., Zhou, W., Vertino, P. M., and Marcus, A. I. (2008) *Cancer Res.* **68,** 740–748
41. Karuman, P., Gozani, O., Odze, R. D., Zhou, X. C., Zhu, H., Shaw, R., Brien, T. P., Bozzuto, C. D., Ooi, D., Cantley, L. C., and Yuan, J. (2001) *Mol. Cell* **7,** 1307–1319
42. Tiainen, M., Ylikorkala, A., and Mäkelä, T. P. (1999) *Proc. Natl. Acad. Sci. U.S.A.* **96,** 9248–9251
43. Belmont, L. D., and Mitchison, T. J. (1996) *Cell* **84,** 623–631
44. Larsson, N., Marklund, U., Gradin, H. M., Brattsand, G., and Gullberg, M. (1997) *Mol. Cell. Biol.* **17,** 5530–5539

Inactivation of chemokine (C-C motif) receptor 1 (CCR1) suppresses colon cancer liver metastasis by blocking accumulation of immature myeloid cells in a mouse model

Takanori Kitamura[a,1], Teruaki Fujishita[a,1], Pius Loetscher[b], Laszlo Revesz[b], Hiroki Hashida[c], Shinae Kizaka-Kondoh[d], Masahiro Aoki[a], and Makoto M. Taketo[a,2]

[a]Department of Pharmacology, Graduate School of Medicine, Kyoto University, Kyoto 606-8501, Japan; [b]Novartis Institutes for BioMedical Research, Novartis Pharma AG, CH-4056 Basel, Switzerland; [c]Department of Gastroenterological Surgery and Oncology, Kitano Hospital, Osaka 530-8480, Japan; and [d]Department of Radiation Oncology and Image-Applied Therapy, Graduate School of Medicine, Kyoto University, Kyoto 606-8507, Japan

Edited by Webster K. Cavenee, Ludwig Institute, University of California-San Diego, La Jolla, CA, and approved June 8, 2010 (received for review February 24, 2010)

Recent reports have suggested critical roles of myeloid cells in tumor invasion and metastasis, although these findings have not led to therapeutics. Using a mouse model for liver dissemination, we show that mouse and human colon cancer cells secrete CC-chemokine ligands CCL9 and CCL15, respectively, and recruit CD34$^+$ Gr-1$^-$ immature myeloid cells (iMCs). They express CCL9/15 receptor CCR1 and produce matrix metalloproteinases MMP2 and MMP9. Lack of the *Ccr1*, *Mmp2*, or *Mmp9* gene in the host dramatically suppresses outgrowths of disseminated tumors in the liver. Importantly, CCR1 antagonist BL5923 blocks the iMC accumulation and metastatic colonization and significantly prolongs the survival of tumor-bearing mice. These results suggest that CCR1 antagonists can provide antimetastatic therapies for patients with disseminated colon cancer in the liver.

chemokine | metalloproteinase | stromal cell

Colon cancer is one of the leading causes of cancer-related deaths (1). Although most primary tumors can be resected surgically, colorectal cancer frequently spreads to the liver, which is responsible for the high mortality of the disease (2). For successful metastasis, cancer cells need to invade surrounding tissues, penetrate microvessels, survive in circulation, disseminate to distant organs, form micrometastases, and expand into macrometastases. To progress through these steps, tumor cells often acquire the capability of survival and invasion by activating metastatic signaling pathways or inactivating metastasis suppressor genes (2, 3). In addition to these cell autonomous changes, tumor stromal cells, especially bone marrow-derived myeloid cells, actively participate in early steps of the metastatic cascade in some mouse models (4). For example, tumor-associated macrophages (TAMs) promote migration and intravasation of mammary tumor cells (5, 6). Bone marrow-derived cells that express myeloid cell marker CD11b and granulocyte marker Gr-1 (CD11b$^+$ Gr-1$^+$) also promote metastasis of breast cancer cells, likely through promotion of intravasation and suppression of immune responses (7). Furthermore, CD11b$^+$ myeloid cells that express vascular endothelial growth factor receptor 1 (VEGFR1) accumulate at the metastatic sites before the arrival of lung cancer and melanoma cells and foster the dissemination of the cancer cells (8). These reports suggest that bone marrow-derived myeloid cells can help cancer epithelium in early steps of metastasis. It remains to be determined whether therapeutics targeting such myeloid cells can prevent cancer metastasis (9).

As a model for invasive colon cancer, we previously constructed *cis-Apc*$^{+/\Delta 716}$ *Smad4*$^{+/-}$ (*Apc/Smad4*) mice that develop intestinal adenocarcinomas with marked invasions by loss of *Apc* and *Smad4* tumor suppressor genes in the intestinal epithelium (10, 11). In the *Apc/Smad4* tumors, we reported that the invading cancer epithelium is associated with immature myeloid cells (iMCs) that express myeloid progenitor cell marker CD34 and CD11b (12). Because these iMCs do not express Gr-1 or VEGFR1, they belong to a different subclass from the Gr-1$^+$ iMCs in breast cancer (7) or VEGFR1$^+$ myeloid cells in pre-metastatic niches (8). Using the *Apc/Smad4* mice, we further showed that the CD34$^+$ Gr-1$^-$ iMCs promote colon cancer invasion into the adjacent tissues (12).

However, whether colon cancer cells in the metastasizing sites can recruit the iMCs like those in the primary sites has not been investigated. Because the intestinal tumors in *Apc/Smad4* mice do not metastasize to the liver or lung during their short lifespan (11), and because no practical models are available whose endogenous (i.e., nontransplant) tumors progress and metastasize to the liver (or lung), here we have resorted to a transplantation model to determine whether colon cancer cells can recruit the iMCs in the metastasizing sites.

Results

Mouse Colon Cancer Cells Disseminated to the Liver Are Associated with iMCs. To investigate possible roles of the CD34$^+$ Gr-1$^-$ iMC subclass in colon cancer metastasis, we injected CMT93 mouse colon cancer cells (Table S1) into the spleen of syngeneic C57BL/6 mice, which allowed efficient dissemination of tumor cells to the liver. We found massive accumulations of stromal cells that expressed CD34, CD11b, and CD45, but not Gr-1 or VEGFR1 (Fig. 1*A* and Fig. S1*A*). We further confirmed that they did not express CD31 (a marker for endothelial cells), CD14 (monocytes), B2.20 (B-cells), CD3ε (T cells), or αSMA (myofibroblasts). These characteristics fit those of the iMC subclass in the primary colon cancer of *Apc/Smad4* mice (12). Of note, some of these stromal cells in the liver expressed macrophage marker F4/80 and dendritic cell marker CD11c that were absent in the *Apc/Smad4* primary tumors (Fig. S1*A*). We also verified their bone marrow-origin by transplanting bone marrow cells containing GFP into irradiated recipients (Fig. S1 *B* and *C*). Based on these results, we concluded that the cancer-associated stromal myeloid cells in the liver belong to the CD34$^+$ Gr-1$^-$ iMC subclass. Further analyses showed that the iMCs started to accumulate at day 7 postinjection when disseminated cancer cells began to form tumor glands. The iMCs accumulated further by day 14 with expansion of the tumor glands in the liver (Fig. 1*B*). By day 21, the

Author contributions: T.K., T.F., M.A., and M.M.T. designed research; T.K. and T.F. performed research; P.L., L.R., H.H., and S.K.-K. contributed new reagents/analytic tools; T.K., T.F., M.A., and M.M.T. analyzed data; and T.K., T.F., M.A., and M.M.T. wrote the paper.

Conflict of interest statement: P.L. and L.R. are employees of Novartis Pharma, AG that holds patents for BL5923.

This article is a PNAS Direct Submission.

[1]T.K. and T.F. contributed equally to this work.

[2]To whom correspondence should be addressed. E-mail: taketo@mfour.med.kyoto-u.ac.jp.

This article contains supporting information online at www.pnas.org/lookup/suppl/doi:10.1073/pnas.1002372107/-/DCSupplemental.

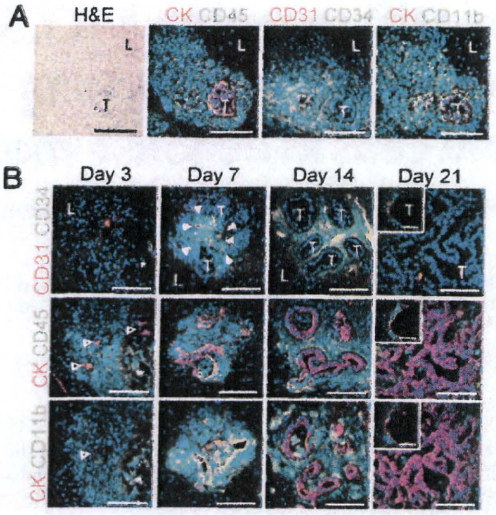

Fig. 1. Accumulation of iMCs around disseminated cancer cells in the liver. (*A*) A metastatic focus in the liver stained with H&E (*Far Left*). Serial sections were immunostained for pan-cytokeratin (CK), CD45, CD31, CD34, and CD11b. T, metastasizing tumor; L, adjacent normal liver. (Scale bars, 100 μm.) (*B*) Liver metastasis foci dissected at days 3, 7, 14, and 21 postinjection. Open arrowheads, disseminated tumor cells; filled arrowheads, a cluster of the iMCs; asterisks, a necrotic area. T, tumor glands; L, adjacent normal liver. (*Insets*) A representative carcinoma cyst. (Scale bars, 100 μm.)

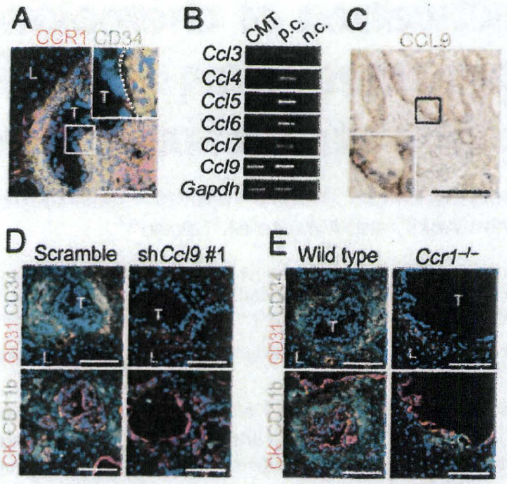

Fig. 2. Inactivation of CCL9-CCR1 signaling blocks accumulation of the iMCs in the liver. (*A*) A metastatic focus in the liver immunostained for CCR1 and CD34. (*Inset*) A higher magnification of the boxed area. T, tumor; L, liver. (Scale bar, 100 μm.) (*B*) Expression of mRNAs for CCR1 ligands determined by RT-PCR. Total RNA was isolated from cultured CMT93 cells. Total RNA from intestinal polyps of *Apc/Smad4* mice was used as a control (p.c.). Negative controls (n.c.) had distilled water instead of RNA. (*C*) A metastatic focus in the liver immunostained for CCL9 (brown DAB staining with hematoxylin counterstaining). (*Inset*) A higher magnification of the boxed area. (Scale bar, 100 μm.) (*D*) Liver metastasis foci in mice injected with CMT93 cells expressing scramble RNA (Scramble) and shRNA against *Ccl9* (sh*Ccl9*#1). Serial sections were immunostained for CK, CD31 and the iMC markers (CD34 and CD11b). T, tumor; L, liver. (Scale bars, 100 μm.) (*E*) Liver metastasis foci in wild-type and *Ccr1*$^{-/-}$ mice injected with CMT93 cells. (Scale bars, 100 μm.)

iMCs disappeared from the metastatic lesions where the cancer cells formed massive glands or carcinoma cysts, suggesting the possibility that the iMCs contributed to an early phase of metastatic expansion. As mentioned above, we could not find VEGFR1^{+} cells in the liver lesions during 2 wk after injection (Fig. S1*A*), although such cells were reported in lung metastatic sites at day 12 after s.c. injection of melanoma cells (8).

Mouse Colon Cancer Cells Secrete CCL9 and Recruit CCR1-Expressing iMCs to the Liver. We next investigated CCR1 expression, another important characteristic of the iMCs. Most iMCs at the metastatic foci expressed CCR1, whereas the cancer epithelium did not (Fig. 2*A*). Because specific ligands activate CCR1 (13) and recruit the iMCs (12), we looked for such ligands that were expressed by the cancer cells. Among them, CMT93 cells expressed only *Ccl9* mRNA but others did not (Fig. 2*B*). Consistently, cultured CMT93 cells secreted CCL9 protein (25 ± 3 pg/10^{5} cells) at a similar level to that by intestinal cancer cells from *Apc/Smad4* polyps (37 ± 16 pg/10^{5} cells). Immunostaining data also confirmed that metastasized CMT93 cells expressed CCL9 but the surrounding stromal cells did not (Fig. 2*C*).

To assess the importance of CCL9 in iMC accumulation in the liver, we prepared CMT93 derivatives that contained shRNA against *Ccl9* or control scramble RNA. Two constructs of the shRNA, sh*Ccl9*#1 and sh*Ccl9*#2, reduced the CCL9 levels to 25% and 47% of control CMT93-scramble cells, respectively (i.e., 7 ± 1, 14 ± 2, and 29 ± 7 pg/10^{5} cells for CMT-sh*Ccl9*#1, CMT-sh*Ccl9*#2, and CMT93-scramble, respectively). As expected, almost all metastatic foci formed by control cells accumulated iMCs markedly. In contrast, such accumulations were not observed in the majority of foci by the CCL9-reduced CMT93 cells (CMT93-sh*Ccl9*#1; Fig. 2*D*). We further injected CMT93 cells into *Ccr1*$^{-/-}$ mice and found that 7 of 10 mice formed no visible metastatic foci in the liver, although the remaining three developed some foci (see below). We therefore examined the minor population of mice for liver metastases, but iMCs were missing around most such lesions (Fig. 2*E*). Collectively, these results suggest that activation of CCR1 by cancer-secreted CCL9 is critical for the iMCs to accumulate at the metastatic foci. As an exception, we found several small metastatic lesions where numerous iMCs accumulated despite the lack of CCR1 (Fig. S2), suggesting a rare alternative mechanism that can recruit iMCs independent of CCR1.

Inactivation of the Mouse CCL9-CCR1 Signaling Blocks Metastatic Expansion of Cancer in the Liver, and Prolongs Host Survival. Because the iMCs helped invasion of primary tumors in the intestines (12), we hypothesized that accumulation of the iMCs could also promote the metastatic expansion of disseminated colon cancer in the liver. We therefore injected luciferase-expressing CMT93 cells into *nu/nu* mice (nude mice), which enabled monitoring of the liver tumors by bioluminescence over time. In mice injected with the parental CMT93 or CMT93-scramble cells, the intensity of bioluminescence began to increase at day 7 postinjection and increased exponentially thereafter (Fig. 3 *A* and *B*). In contrast, such an increase in luminescence was markedly suppressed in mice injected with CMT93-sh*Ccl9*#1 cells, although they showed essentially the same levels of luminescence as control groups up to day 3. Another shRNA construct (sh*Ccl9*#2) showed a similar effect, although at a weaker level than that of sh*Ccl9*#1 (Fig. 3*B*). Of note, all CMT93 derivatives showed essentially the same luciferase activity and proliferation rate in culture. We then injected luciferase-expressing CMT93 cells into the wild-type and *Ccr1*$^{-/-}$ mice. Although all wild-type mice showed marked increases in the luminescence level at day 14 postinjection, such an increase was not observed in 70% (7/10) of *Ccr1*$^{-/-}$ mice (Fig. 3*C*). In these hosts, we did not find any macroscopic foci on liver surfaces (Fig. 3*D*). These results indicate that accumulation of the iMCs via CCL9-CCR1 axis plays a major role in the expansion of liver metastasis foci. Although all mice injected with the CMT93-scramble or parental cells became moribund within 54 d, 60% (3/5) and 20% (2/10) of mice injected with CMT93-sh*Ccl9* #1 and CMT93-sh*Ccl9* #2 cells, respectively,

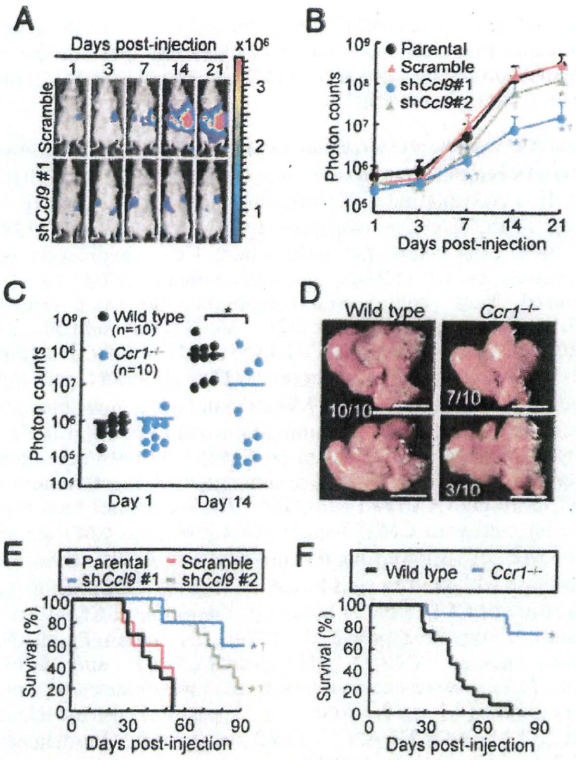

Fig. 3. Blockade of CCL9-CCR1 signaling suppresses expansion of metastatic lesions and prolongs host survival. (*A*) Representative in vivo bioluminescence images of mice injected with luciferase-expressing CMT93 cells that contained scramble RNA (*Upper*) or shRNA against *Ccl9* (*Lower*). Colored scale bar represents intensity of bioluminescence in photons/sec. (*B*) Quantification of metastatic lesions by bioluminescence (photon counts) from luciferase-expressing CMT93 cells (Parental), or their derivatives that contained scramble RNA (Scramble) or shRNA against *Ccl9* (sh*Ccl9*#1 or sh*Ccl9*#2). Results are given as the means ± SD $^{*}P < 0.02$ and $^{\dagger}P < 0.02$ compared with Parental and Scramble, respectively (n = 8–11 mice in each group). (*C*) Quantification of metastatic lesions by bioluminescence from luciferase-expressing CMT93 cells injected into wild-type and *Ccr1*$^{-/-}$ mice. Each circle represents an individual mouse. Horizontal lines show the means of the respective groups. $^{*}P < 0.01$. (*D*) Representative macroscopic views of the liver dissected from wild-type and *Ccr1*$^{-/-}$ mice injected with CMT93 cells. (Scale bars, 10 mm.) (*E*) Kaplan-Meier plot showing survival of wild-type hosts injected with control CMT93 cells (Prnt and Scr) or those containing shRNA constructs against *Ccl9* (sh*Ccl9*#1 or sh*Ccl9*#2). $^{*}P < 0.01$ and $^{\dagger}P < 0.02$ compared with Prnt and Scr, respectively (n = 5–10 mice in each group). (*F*) Survival rates of wild-type and *Ccr1*$^{-/-}$ mice injected with parental CMT93 cells. $^{*}P = 0.0001$(n = 12–13 mice in each group).

remained alive till the end of analysis (day 90; Fig. 3*E*). Likewise, 75% (9/12) of the tumor-transplanted *Ccr1*$^{-/-}$ mice survived to day 90, in contrast to the wild type that became moribund before day 75 (Fig. 3*F*). These results indicate that inactivation of the CCL9-CCR1 signaling prolongs the survival by blocking early metastatic expansion.

Lack of MMP2 or MMP9 in the Host Mouse Suppresses Expansion of Metastatic Lesions in the Liver. For metastatic expansion in the liver, disseminated cancer cells need to invade the liver parenchyma. We therefore hypothesized that the iMCs promote intrahepatic invasion of disseminated cancer through secretion of proteases. To identify such enzymes, we compared mRNA levels in the metastatic foci between the wild-type and *Ccr1*$^{-/-}$ mice by microarray and RT-PCR (Fig. S3*A*). The results showed more than twofold increases in the levels of *Mmp2*, *Mmp7*, *Mmp9*, and *Mmp13* in the iMC-associated foci in wild-type mice (Fig. S3*B*). In such lesions, MMP2 and MMP9 were expressed in the stromal iMCs, but not in the cancer epithelium (Fig. 4 *A* and *B*), whereas MMP7 and MMP13 were found primarily in the epithelium (Fig. S3*C*). Consistently, MMP2 and MMP9 were absent around the liver foci in *Ccr1*$^{-/-}$ mice where the iMCs were missing, although MMP7 and MMP13 were present (Fig. 4*A* and Fig. S3*C*). We then injected luciferase-expressing CMT93 cells into *Mmp2*$^{-/-}$ mice and found significant reduction in the liver luminescence at day 14, compared with those in *Mmp2*$^{+/+}$ littermates (Fig. 4*C*). Likewise, the luciferase luminescence was much lower in *Mmp9*$^{-/-}$ mice than *Mmp9*$^{+/+}$ littermates, whereas such a reduction was not observed in *Mmp7*$^{-/-}$ mice (Fig. 4*C*). Notably, almost all metastatic foci in the *Mmp2*$^{-/-}$ and *Mmp9*$^{-/-}$ mice consisted of smaller cancer glands than those in wild-type mice, although they were associated with the iMCs (Fig. 4*D*). These results suggest that MMP2 and MMP9 are critical for the iMCs to promote metastatic expansion of colon cancer cells, but not to accumulate in the liver.

Some Human Colon Cancer Cells Express CCR1 Ligand CCL15. To test whether human colon cancer cells could recruit iMCs, we injected four cell lines into the spleen of *nu/nu* mice and found that HT29 cells were associated with the iMCs in the liver, whereas HCT116, DLD-1, or SW620 cells were not (Fig. 5*A* and Fig. S4*A*). Based on the structural similarity, human orthologs of mouse CCL9 have been suspected to be CCL15 and/or CCL23 (14–16). Thus, we

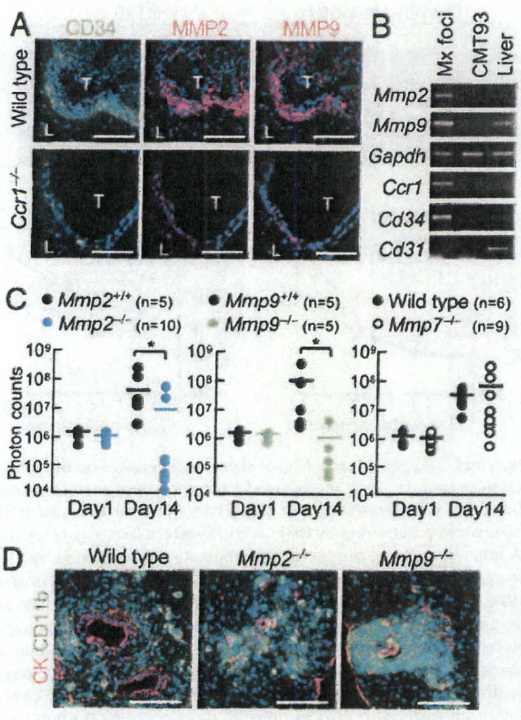

Fig. 4. Lack of MMP2 or MMP9 inhibits expansion of metastatic liver lesions. (*A*) Liver metastasis foci from wild-type and *Ccr1*$^{-/-}$ mice injected with CMT93 cells. Serial sections were stained for CD34, MMP2, and MMP9. T, tumor; L, liver. (Scale bars, 100 μm.) (*B*) Expression of MMP mRNAs determined by RT-PCR. Total RNA was isolated from metastatic foci in wild-type mice (Mx foci), cultured CMT93 cells, and normal mouse liver. Expression of mRNAs for CCR1, CD34, and CD31 were also determined. (*C*) Quantification of metastatic lesions by bioluminescence from luciferase-expressing CMT93 cells. Each circle represents an individual mouse. Horizontal lines show the means of the respective groups. $^{*}P < 0.01$ (n = 9–11 mice in each group). (*D*) Liver metastasis foci in wild-type, *Mmp2*$^{-/-}$, and *Mmp9*$^{-/-}$ mice injected with CMT93 cells. (Scale bars, 100 μm.)

determined the levels of these chemokines in 11 human colon cancer cell lines, and found that six of them including HT29 expressed *CCL15* mRNA and protein at high levels, but not *CCL23* (Fig. 5*B*, Fig. S4 *B* and *C*, and Table S1). We could not detect mRNAs for any other CCR1 ligands; CCL3, 4, 5, 7, 14, or 16 (Fig. S4*C*). We further verified by Western blotting that 28% (13/47) of human colon cancer specimens expressed CCL15 protein (Fig. 5*C*). An immunostaining analysis also showed that 29% (12/41) of primary tumors and 29% (12/41; a separate combination) of liver metastases expressed CCL15 in the cancer epithelium (Fig. 5*D*). These results demonstrate that a subset of human colon cancer cases secretes CCL15 and suggest that it may recruit CCR1$^+$ human iMCs.

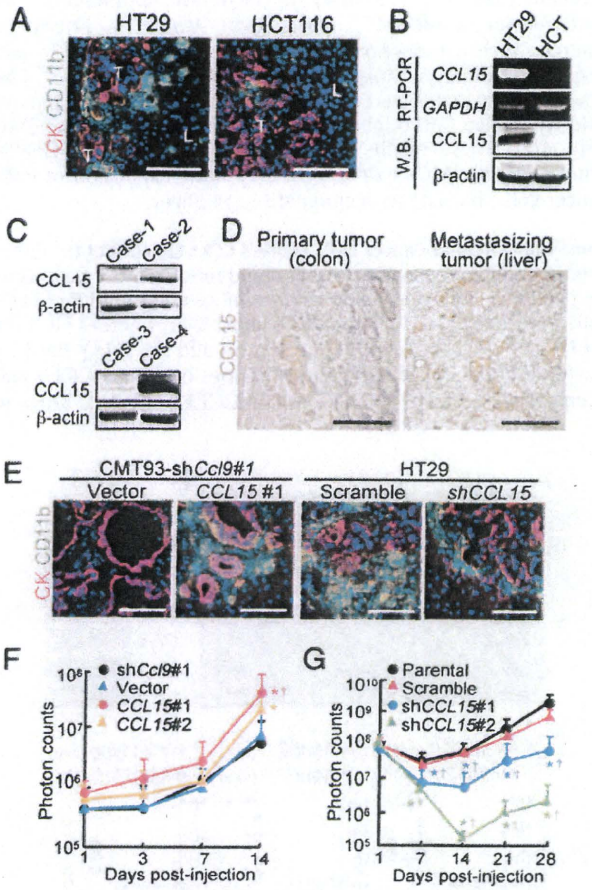

Fig. 5. Human CCL15 recruits the iMCs and promotes expansion of metastatic lesions in mouse liver. (*A*) Liver metastasis foci formed by human colon cancer cells HT29 and HCT116. T, tumor; L, liver. (Scale bars, 100 μm.) (*B*) Levels of CCL15 mRNA and protein determined by RT-PCR and Western blotting, respectively. Total RNA and lysates were prepared from metastatic foci formed by the human colon cancer cell lines in mouse liver. (*C*) Determination of CCL15 protein levels by Western blotting. Lysates were prepared from human colon cancer specimens. Cases-2 and 4 expressed CCL15. β-actin was used as a loading control. (*D*) Human colon cancer specimens immunostained for CCL15 (hematoxylin counterstaining). Tumors were dissected from the primary (colon) and metastatic (liver) sites of the same patients. (Scale bars, 100 μm.) (*E*) Liver metastasis foci from mice with CMT93-sh*Ccl9*#1 cells containing empty vector (Vector) or the *CCL15* gene (*CCL15*#1) (*Left*), and with HT29 cells expressing scramble RNA (HT29-scramble) or shRNA against *CCL15* (HT29-sh*CCL15*) (*Right*). (Scale bars, 100 μm.) (*F*) Quantification of the metastatic lesions in mice injected with CMT93-sh*Ccl9* cells (sh*Ccl9*#1), or their derivatives with empty (Vector) or CCL15-expressing vector (*CCL15*#1 or *CCL15*#2). Results are given as the means ± SD $^*P < 0.04$ and $^\dagger P < 0.03$ compared with sh*Ccl9*#1 and Vector, respectively (n = 5–19 mice in each group). Note that the ordinate is in a logarithmic scale. (*G*) Quantification of the metastatic lesions in mice injected with luciferase-expressing HT29 cells (Parental), or their derivatives expressing scramble RNA (Scramble) or shRNA constructs against *CCL15* (sh*CCL15*#1 or sh*CCL15*#2). Results are given as the means ± SD $^*P < 0.04$ and $^\dagger P < 0.04$ compared with Parental and Scramble, respectively (n = 6–12 mice in each group).

Human CCL15 Promotes Accumulation of the iMCs and Expansion of Metastatic Foci in Mouse Liver. To assess the role of human CCL15 in iMC accumulation and following metastatic expansion of cancer in the liver, we constructed derivatives of the CMT93-sh*Ccl9*#1 cells where not only mouse CCL9 expression was suppressed by an shRNA, but also human *CCL15* was introduced. These cells secreted essentially the same level of CCL15 as those by HT29 cells (321 ± 16, 315 ± 34, and 302 ± 18 pg/10^5 cells for CMT-sh*Ccl9*:CCL15#1, CMT-sh*Ccl9*:CCL15#2, and HT29, respectively), whereas CMT93-sh*Ccl9*#1 cells with the empty vector (CMT-sh*Ccl9*:Vector) did not at any detectable levels. As expected, iMC accumulation was blocked in the majority of metastatic foci formed by CMT93-sh*Ccl9*:Vector cells. In contrast, numerous iMCs accumulated in most tumors of CMT93-sh*Ccl9*:CCL15#1 cells (Fig. 5*E*). We further found that mice injected with CMT93-sh*Ccl9*:CCL15#1 and CMT-sh*Ccl9*:CCL15#2 cells showed higher luminescence levels in the liver than those with control cells at day 14 (Fig. 5*F*). Of note, forced expression of CCL15 did not affect proliferation of CMT93 cells in culture. We next prepared HT29 cells containing shRNA against human *CCL15* (HT29-sh*CCL15*#1 and HT29-sh*CCL15*#2) where expression of CCL15 was reduced to a negligible level (0.1 ± 0.2 and 4 ± 3 pg/10^5 cells for HT29-sh*CCL15*#1 and HT29-sh*CCL15*#2, respectively). In metastatic foci formed by HT29-sh*CCL15*#1 cells, accumulation of the iMCs was markedly reduced compared with those by HT29-scramble cells (Fig. 5*E*). Furthermore, shRNA against *CCL15* (sh*CCL15*#1 and sh*CCL15*#2) significantly reduced the luminescence levels in mice injected with HT29 cells (Fig. 5*G*). These results indicate that CCL15 secreted from human colon cancer cells can recruit mouse CCR1$^+$ iMCs, and promote their metastatic expansion.

CCR1 Antagonist BL5923 Blocks Metastatic Expansion of Cancer in the Mouse Liver and Prolongs Host Survival. Finally, we evaluated a CCR1 antagonist for its suppressive effects on colon cancer metastasis in the mouse liver dissemination model. We administered BL5923 (ref. 17, and *SI Methods*) or the vehicle to *v/v* mice that were injected with mouse (CMT93) or human (HT29) colon cancer cells as described above. Treatment of the host mice with 50 mg/kg of BL5923, but not the vehicle, markedly reduced the accumulation of iMCs around the metastatic foci of CMT93 as well as HT29 (Fig. 6*A*). In mice injected with the luciferase-expressing CMT93 cells, BL5923 (at 50 mg/kg) significantly reduced the luminescence levels at day 14, compared with the markedly increased levels in the vehicle-treated mice (Fig. 6*B* and Fig. S5*A*). A lower dose of the compound (25 mg/kg) was ineffective to block the metastatic expansion. As anticipated, BL5923 did not affect the proliferation rate of CMT93 cells in culture (Fig. S5*B*). Likewise, expansion of HT29 cells in the liver was significantly blocked by treatment with 50 mg/kg of BL5923 (Fig. 6*C* and Fig. S5*C*). In contrast, it did not suppress the metastatic expansion of HCT116 cells that could form metastases without iMC accumulation (Figs. 5*A* and 6*C*), consistent with the mechanism that BL5923 blocks tumor metastasis through CCR1 inhibition in the iMCs. We further found that the BL5923 treatment prolonged the mean survival of the hosts from 37 d postinjection to 62 d and from 84 d to 113 d when CMT93 and HT29 cells were injected, respectively (Fig. 6 *D* and *E*). These results strongly suggest that CCR1 antagonist BL5923 suppresses accumulation of the iMCs and early metastatic expansion of colon cancer, allowing the prolonged host survival.

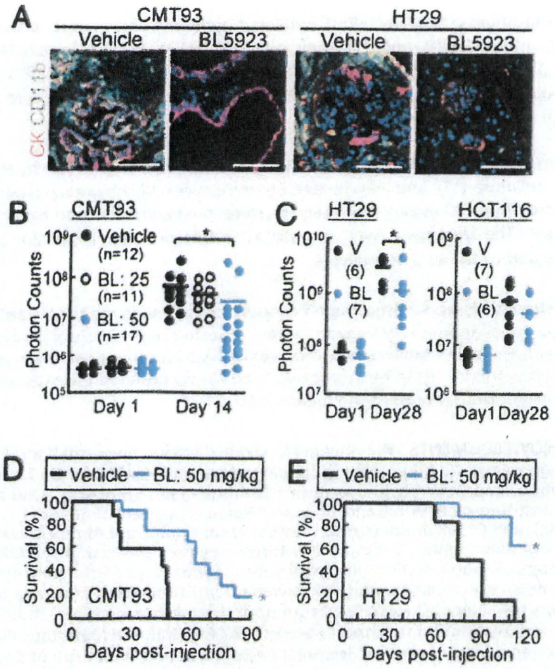

Fig. 6. CCR1 antagonist BL5923 blocks expansion of metastatic lesions and prolongs host survival. (*A*) Liver metastasis foci from mice treated with vehicle or BL5923 (50 mg/kg). Mice were injected with CMT93 cells (*Left*) or HT29 cells (*Right*). (Scale bars, 100 μm.) (*B*) Quantification of metastatic lesions in mice injected with CMT93 cells, and treated with the vehicle or BL5923 at 20 or 50 mg/kg (BL: 25 or BL: 50, respectively). Each circle represents an individual mouse. Horizontal lines show the means of the respective groups. $*P < 0.01$ compared with Vehicle (n = 11–17 mice in each group). (*C*) Quantification of the metastatic lesions in mice treated with vehicle (V) or 50 mg/kg of BL5923 (BL). Mice were injected with HT29 (*Left*) or HCT116 (*Right*) cells. Each circle represents an individual mouse. Horizontal lines show the means of the respective groups. $*P < 0.04$ compared with vehicle (n = 6–7 mice in each group). (*D* and *E*) Kaplan-Meier plots showing survivals of the host mice treated with the vehicle or BL5923 (BL: 50 mg/kg). Mice were injected with CMT93 (*D*) or HT29 (*E*). $*P = 0.004$ compared with vehicle (n = 7–11 mice in each group).

Discussion

In the mouse model, we have found that colon cancer cells disseminated to the liver begin to form micrometastases by day 7 postinjection and rapidly expand thereafter mirroring the extent of iMC accumulation (Figs. 1*B* and 3*B*). Because the disseminated cancer cells cannot expand when the iMC accumulation is blocked, these results suggest that the $CD34^+$ $Gr\text{-}1^-$ iMCs promote a late step of the metastatic cascade: expansion of disseminated cancer and colonization. Because the iMCs have disappeared by day 21 postinjection when cancer cells colonize in the liver, they may support an early phase of metastatic expansion that is rate limiting in the metastatic cascade (18). Consistently, suppression of such early metastatic expansion prolongs survival of mice with disseminated colon cancer in the liver. On the other hand, different subclasses of myeloid cells such as TAMs and $Gr\text{-}1^+$ iMCs help breast cancer cells to invade microvessels, an early step of the metastatic cascade (5–7). However, the $CD34^+$ $Gr\text{-}1^-$ iMCs appear to have only a minor role, if any, in the intravasation and dissemination because the primary colon cancer in *Apc/Smad4* mice do not metastasize despite marked accumulation of the iMCs at the invasion fronts and strong local invasion (10–12).

Interestingly, we have found that CMT93 mouse colon cancer cells recruit the iMCs from the bone marrow to metastatic lesions through the same mechanism as that underlying recruitment of the cells to the primary tumors, activation of CCR1 on the iMCs. Like intestinal tumor epithelium of *Apc/Smad4* mice (12), CMT93 colon cancer cells secrete CCL9, a CCR1 ligand and strong chemoattractant for bone marrow cells (19). Because CMT93 cells do not express other CCR1 ligands (CCL3-CCL7), CCL9 appears to be the only ligand that plays a critical role in recruiting the iMCs. Although human ortholog of mouse CCL9 has not been identified, we have shown here that one-third of human colon cancer metastases express CCL15 that has a structural similarity with CCL9 (14–16). We have further demonstrated that HT29 human colon cancer cells secrete CCL15, recruit mouse iMCs, and expand in the liver, whereas the CCL15-reduced HT29 cells fail to do so. These results suggest that CCL15 secreted from human colon cancer plays a critical role in the recruitment of bone marrow-derived iMCs as a functional homolog of mouse CCL9. Consistently, human CCL15 can promote in vitro migration of mouse mononuclear cells isolated from the bone marrow (20). Although we have been unable to detect CCR1-expressing bone marrow-derived cells in clinical specimens of colon cancer metastasis, it is likely because access is limited only to those in late stages. The transient nature of iMC accumulation in metastasis remains to be investigated further.

In our liver metastasis model, we have found that the iMCs express MMP2 and MMP9, but the tumor epithelium does not. These results are consistent with previous reports that show stroma-restricted expression of the MMPs in human liver metastases of colorectal cancer (21, 22). Abundant expression of MMP2 or MMP9 is associated with poor prognosis and high mortality of colon cancer patients (23–27). Although selective inhibitors of MMP2/9 significantly block mouse liver metastasis of colon cancer and prolong the survival of tumor-bearing mice (28), clinical trials for MMP inhibitors have failed because of severe side effects such as musculoskeletal pain and inflammation (29–31). Alternatively, we have shown here in a mouse model that reduced iMC accumulation by inactivation of CCR1 can suppress metastatic expansion of colon cancer. These results provide the rationale for application of CCR1 antagonists to colon cancer treatment that targets the MMP-expressing myeloid cells, rather than direct and systemic inhibition of MMPs (32). Supporting this novel strategy of "cellular target therapy" (12), we have demonstrated here that CCR1 antagonist BL5923 significantly blocks liver metastasis of mouse (CMT93) and human (HT29) colon cancer cells and prolongs the host survival. Because $Ccr1^{-/-}$ mice are healthy unless challenged with specific pathogens (33), therapeutic inactivation of CCR1 may exhibit few side effects. Consistently, several CCR1 antagonists were well tolerated in phase II trials for rheumatoid arthritis and multiple sclerosis (34). It is therefore possible that administration of CCR1 antagonists as an adjuvant therapy after surgical resection of the primary tumors can improve the survival of patients with colorectal cancer that expresses CCL15. Our present results await clinical trials for such therapies.

Methods

Mice. C57BL/6, $Ccr1^{-/-}$ (33), $Mmp2^{-/-}$ (35), $Mmp7^{-/-}$ (36), $Mmp9^{-/-}$ (37), and *nu/nu* mice at 7 wk of age were used as hosts of tumor injections (see below). All animals were bred and maintained according to the protocol approved by the Animal Care and Use Committee of Kyoto University. Genetic background and origin of the mice are detailed in *SI Methods*.

Cell Lines. CMT93 mouse colon cancer cells (derived from C57BL/6 strain), HT29, DLD-1, SW620, and HCT116 human colon cancer cells were cultured at 37 °C under 5% CO_2 in DMEM with 10% FCS. These cells were transfected with expression vectors encoding luciferase or CCL15, or shRNA expression vectors targeting *Ccl9* and *CCL15* (*SI Methods*).

Clinical Samples. Colon cancer samples for Western blotting were prepared from primary tumors of 47 patients who underwent operations with in-

formed consents. For immunostaining, we prepared an additional 41 sets of the primary colon cancers and liver metastases derived from the same patients.

Experimental Metastasis Model. We injected 1.5×10^6 of CMT93 cells into the spleens of C57BL/6 or knockout mice (C57BL/6 backgrounds) under anesthesia. We also injected 1×10^6 of CMT93 or 3×10^6 of human cancer cells into *nu/nu* mice (*SI Methods*). The spleen was removed 1 min after tumor injection to prevent splenic tumor formation, so that metastatic lesions developed only in the liver.

In Vivo Bioluminescence Imaging. We injected 100 μL of D-luciferin solution (10 mg/mL in PBS, i.p.; Promega) into anesthetized tumor-bearing mice 15 min before imaging. Bioluminescence from the luciferase-expressing tumor cells was determined at days 1, 3, 7, 14, 21, and 28 postinjection, using IVIS-SPECTRUM in vivo photon-counting device (Caliper Life Sciences). Images were quantified as photon counts/second using the Living Image software (Caliper Life Sciences).

Histological Analyses. The methods used for immunostaining were based on those previously described (12). Details are given in *SI Methods*.

Western Blotting. Lysates (50 μg protein each) were separated in 10–20% gradient SDS-gels (WAKO), and Western blotting was performed as described previously (38). CCL15 was detected with a goat polyclonal antibody for human CCL15 (R&D) and Qentix Western Blot Signal Enhancer (Pierce).

RT-PCR. Expression of mRNAs was determined by RT-PCR as described previously (12). Primer sequences are shown in *SI Methods*.

Quantifications of CCL9 and CCL15 Proteins. Conditioned media were collected from cultured CMT93 and HT29 cells, and their derivatives. The levels of CCL9 (MIP-1γ), and CCL15 (MIP-1δ) were determined using the Mouse MIP-1γ Immunoassay Kit, and Human CCL15/MIP-1δ DuoSet ELISA Development Kit (R&D), respectively.

Drug Treatment. BL5923 (Novartis) was dissolved in 0.5% (wt/vol) hydroxyethyl cellulose (17), and administered to mice twice daily by oral gavages at doses of 25 or 50 mg/kg. The relevant solvent was administered to control animals. The treatments were started at 3 d before tumor injection, and continued to the end of analyses.

Statistical Analyses. Statistical significance was evaluated with the Student's *t* test or nonparametric Wilcoxon *u* test. The log-rank test was used for analysis of Kaplan-Meier survival curves. All statistical analyses were performed with JMP 7 (SAS Institute). $P < 0.05$ was considered as statistically significant. Data represent the means ± SD.

ACKNOWLEDGMENTS. We thank M. Okabe (Osaka University) for EGFP transgenic mice, P. M. Murphy (National Institutes of Health) for *Ccr1* knockout mice, and Z. Werb (University of California, San Francisco), S. Itohara [The Institute of Physical and Chemical Research (Japan) Brain Science Institute], and C. Takahashi (Kyoto University) for *Mmp2* and *Mmp9* knockout mice. We also thank T. Inai and E. Hirose (Kyushu University) for CMT93 subtypes, T. Sudo (TORAY Industries Inc., Tokyo, Japan) for performing DNA microarray analysis, and Dr. Kawada (Kyoto University) for preparing human specimens. This work was supported by the Jeannik M. Littlefield-American Association for Cancer Research (AACR) Grants in Metastatic Colon Cancer and Grant-in Aid for Scientific Research from the Ministry of Education, Culture, Sports and Technology of Japan (to M.M.T).

1. Jemal A, et al. (2008) Cancer statistics, 2008. *CA Cancer J Clin* 58:71–96.
2. Christofori G (2006) New signals from the invasive front. *Nature* 441:444–450.
3. Smith SC, Theodorescu D (2009) Learning therapeutic lessons from metastasis suppressor proteins. *Nat Rev Cancer* 9:253–264.
4. Joyce JA, Pollard JW (2009) Microenvironmental regulation of metastasis. *Nat Rev Cancer* 9:239–252.
5. Goswami S, et al. (2005) Macrophages promote the invasion of breast carcinoma cells via a colony-stimulating factor-1/epidermal growth factor paracrine loop. *Cancer Res* 65:5278–5283.
6. Wyckoff JB, et al. (2007) Direct visualization of macrophage-assisted tumor cell intravasation in mammary tumors. *Cancer Res* 67:2649–2656.
7. Yang L, et al. (2008) Abrogation of TGF β signaling in mammary carcinomas recruits Gr-1+CD11b+ myeloid cells that promote metastasis. *Cancer Cell* 13:23–35.
8. Kaplan RN, et al. (2005) VEGFR1-positive haematopoietic bone marrow progenitors initiate the pre-metastatic niche. *Nature* 438:820–827.
9. Gadea BB, Joyce JA (2006) Tumour-host interactions: Implications for developing anticancer therapies. *Expert Rev Mol Med* 8:1–32.
10. Takaku K, et al. (1998) Intestinal tumorigenesis in compound mutant mice of both *Dpc4* (*Smad4*) and *Apc* genes. *Cell* 92:645–656.
11. Taketo MM, Edelmann W (2009) Mouse models of colon cancer. *Gastroenterology* 136:780–798.
12. Kitamura T, et al. (2007) SMAD4-deficient intestinal tumors recruit CCR1$^+$ myeloid cells that promote invasion. *Nat Genet* 39:467–475.
13. Balkwill F (2004) Cancer and the chemokine network. *Nat Rev Cancer* 4:540–550.
14. Wang W, Bacon KB, Oldham ER, Schall TJ (1998) Molecular cloning and functional characterization of human MIP-1 δ, a new C-C chemokine related to mouse CCF-18 and C10. *J Clin Immunol* 18:214–222.
15. Zlotnik A, Morales J, Hedrick JA (1999) Recent advances in chemokines and chemokine receptors. *Crit Rev Immunol* 19:1–47.
16. Forssmann U, Mägert H-J, Adermann K, Escher SE, Forssmann W-G (2001) Hemofiltrate CC chemokines with unique biochemical properties: HCC-1/CCL14a and HCC-2/CCL15. *J Leukoc Biol* 70:357–366.
17. Revesz L, et al. (2006) Bridged piperazines and piperidines as CCR1 antagonists with oral activity in models of arthritis and multiple sclerosis. *Lett Drug Des Discov* 3:689–694.
18. Chambers AF, Groom AC, MacDonald IC (2002) Dissemination and growth of cancer cells in metastatic sites. *Nat Rev Cancer* 2:563–572.
19. Yang M, Odgren PR (2005) Molecular cloning and characterization of rat CCL9 (MIP-1γ), the ortholog of mouse CCL9. *Cytokine* 31:94–102.
20. Kominsky SL, Abdelmagid SM, Doucet M, Brady K, Weber KL (2008) Macrophage inflammatory protein-1 δ: A novel osteoclast stimulating factor secreted by renal cell carcinoma bone metastasis. *Cancer Res* 68:1261–1266.
21. Théret N, et al. (1997) Overexpression of matrix metalloproteinase-2 and tissue inhibitor of matrix metalloproteinase-2 in liver from patients with gastrointestinal adenocarcinoma and no detectable metastasis. *Int J Cancer* 74:426–432.
22. Zeng ZS, Guillem JG (1995) Distinct pattern of matrix metalloproteinase 9 and tissue inhibitor of metalloproteinase 1 mRNA expression in human colorectal cancer and liver metastases. *Br J Cancer* 72:575–582.
23. Cho YB, et al. (2007) Matrix metalloproteinase-9 activity is associated with poor prognosis in T3-T4 node-negative colorectal cancer. *Hum Pathol* 38:1603–1610.
24. Hilska M, et al. (2007) Prognostic significance of matrix metalloproteinases-1, -2, -7 and -13 and tissue inhibitors of metalloproteinases-1, -2, -3 and -4 in colorectal cancer. *Int J Cancer* 121:714–723.
25. Sutnar A, et al. (2007) Clinical relevance of the expression of mRNA of MMP-7, MMP-9, TIMP-1, TIMP-2 and CEA tissue samples from colorectal liver metastases. *Tumour Biol* 28:247–252.
26. Langers AMJ, et al. (2008) MMP-2 geno-phenotype is prognostic for colorectal cancer survival, whereas MMP-9 is not. *Br J Cancer* 98:1820–1823.
27. Inafuku Y, et al. (2009) Matrix metalloproteinase-2 expression in stromal tissues is a consistent prognostic factor in stage II colon cancer. *Cancer Sci* 100:852–858.
28. Wagenaar-Miller RA, Gorden L, Matrisian LM (2004) Matrix metalloproteinases in colorectal cancer: Is it worth talking about? *Cancer Metastasis Rev* 23:119–135.
29. Coussens LM, Fingleton B, Matrisian LM (2002) Matrix metalloproteinase inhibitors and cancer: Trials and tribulations. *Science* 295:2387–2392.
30. Egeblad M, Werb Z (2002) New functions for the matrix metalloproteinases in cancer progression. *Nat Rev Cancer* 2:161–174.
31. Overall CM, Kleifeld O (2006) Tumour microenvironment—opinion: Validating matrix metalloproteinases as drug targets and anti-targets for cancer therapy. *Nat Rev Cancer* 6:227–239.
32. Kitamura T, Taketo MM (2007) Keeping out the bad guys: Gateway to cellular target therapy. *Cancer Res* 67:10099–10102.
33. Gao J-L, et al. (1997) Impaired host defense, hematopoiesis, granulomatous inflammation and type 1-type 2 cytokine balance in mice lacking CC chemokine receptor 1. *J Exp Med* 185:1959–1968.
34. Ribeiro S, Horuk R (2005) The clinical potential of chemokine receptor antagonists. *Pharmacol Ther* 107:44–58.
35. Itoh T, et al. (1997) Unaltered secretion of β-amyloid precursor protein in gelatinase A (matrix metalloproteinase 2)-deficient mice. *J Biol Chem* 272:22389–22392.
36. Wilson CL, Heppner KJ, Labosky PA, Hogan BLM, Matrisian LM (1997) Intestinal tumorigenesis is suppressed in mice lacking the metalloproteinase matrilysin. *Proc Natl Acad Sci USA* 94:1402–1407.
37. Vu TH, et al. (1998) MMP-9/gelatinase B is a key regulator of growth plate angiogenesis and apoptosis of hypertrophic chondrocytes. *Cell* 93:411–422.
38. Fujishita T, Aoki K, Lane HA, Aoki M, Taketo MM (2008) Inhibition of the mTORC1 pathway suppresses intestinal polyp formation and reduces mortality in ApcDelta716 mice. *Proc Natl Acad Sci USA* 105:13544–13549.

Cancer Cell
Article

Suppression of Colon Cancer Metastasis by Aes through Inhibition of Notch Signaling

Masahiro Sonoshita,[1,7] Masahiro Aoki,[1,7,9] Haruhiko Fuwa,[2] Koji Aoki,[1] Hisahiro Hosogi,[1,3] Yoshiharu Sakai,[3] Hiroki Hashida,[4] Arimichi Takabayashi,[4] Makoto Sasaki,[2] Sylvie Robine,[5] Kazuyuki Itoh,[6] Kiyoko Yoshioka,[6] Fumihiko Kakizaki,[1] Takanori Kitamura,[1] Masanobu Oshima,[1,8] and Makoto Mark Taketo[1,*]

[1]Department of Pharmacology, Graduate School of Medicine, Kyoto University, Kyoto 606-8501, Japan
[2]Laboratory of Biostructural Chemistry, Graduate School of Life Sciences, Tohoku University, Sendai 981-8555, Japan
[3]Department of Surgery, Graduate School of Medicine, Kyoto University, Kyoto 606-8501, Japan
[4]Department of Gastroenterological Surgery and Oncology, Kitano Hospital, Osaka 530-8480, Japan
[5]Equipe de Morphogenèse et Signalisation cellulaires, Institut Curie, 75248 Paris, France
[6]Department of Biology, Osaka Medical Center for Cancer and Cardiovascular Diseases, Osaka 537-8511, Japan
[7]These authors contributed equally to this work
[8]Present address: Division of Genetics, Center for Cancer and Stem Cell Research, Kanazawa University, Kanazawa 920-0934, Japan
[9]Division of Molecular Pathology, Aichi Cancer Center Research Institute, Nagoya 464-8681, Japan
*Correspondence: taketo@mfour.med.kyoto-u.ac.jp
DOI 10.1016/j.ccr.2010.11.008

SUMMARY

Metastasis is responsible for most cancer deaths. Here, we show that *Aes* (or *Grg5*) gene functions as an endogenous metastasis suppressor. Expression of Aes was decreased in liver metastases compared with primary colon tumors in both mice and humans. Aes inhibited Notch signaling by converting active Rbpj transcription complexes into repression complexes on insoluble nuclear matrix. In tumor cells, Notch signaling was triggered by ligands on adjoining blood vessels, and stimulated transendothelial migration. Genetic depletion of *Aes* in $Apc^{\Delta 716}$ intestinal polyposis mice caused marked tumor invasion and intravasation that were suppressed by Notch signaling inhibition. These results suggest that inhibition of Notch signaling can be a promising strategy for prevention and treatment of colon cancer metastasis.

INTRODUCTION

Most cancer patients die of metastasis. Although there have been substantial advances in our understanding of the mechanisms of cancer metastasis, efficient remedies for prevention and treatment of metastasis are still missing. The invasion-metastasis cascade consists of local invasion, intravasation, transport, extravasation, formation of micrometastases, and colonization (Fidler, 2003; Steeg, 2006). This sequence is completed only infrequently, causing metastatic inefficiency, and the least efficient of these steps appears to be colonization (Smith and Theodorescu, 2009). Spread of metastatic cancer cells via blood circulation is responsible for the majority of distant metastases, although they may travel also through the lymph ducts to nodes (Weinberg, 2007). In colorectal cancer, metastatic tropism to the liver and lungs can be explained largely by the organization of venous circulation of the intestines through portal vein to the liver, and further to the lungs through pulmonary artery.

Among endogenous colon tumor models, the widely used *Apc* (*Adenomatous polyposis coli*) mutant mice form adenomas in the small intestine, with wide multiplicities (3–300 per animal) depending on the mutational allele, although several adenomas are also found in the colon (Taketo and Edelman, 2009). Additional mutations introduced into *Apc* mutant mice can modify the tumor phenotype. For example, knocking out *Smad4* gene in the TGF-β family signaling converts the benign intestinal adenomas to very invasive adenocarcinomas (Takaku et al.,

Significance

We have found that Aes suppresses colon cancer metastasis by inhibiting Notch signaling pathway. The molecular mechanism of Notch inhibition is through transcriptional repression by sequestering Rbpj, NICD, and Maml1 to nuclear matrix. The cellular mode of metastasis suppression includes inhibition of transendothelial migration (TEM) of tumor cells, which blocks intravasation. Heterotypic interaction between cancer and host cells activates Notch signaling and promotes TEM of metastasizing cancer cells. Because TEM in metastasis is common to many solid tumors, this mechanism is important in various types of cancers. As a model for colon cancer invasion and intravasation, compound mutant mice for the *Apc* and *Aes* genes should be useful to evaluate upcoming therapeutics including Notch signaling inhibitors against colon cancer metastasis.

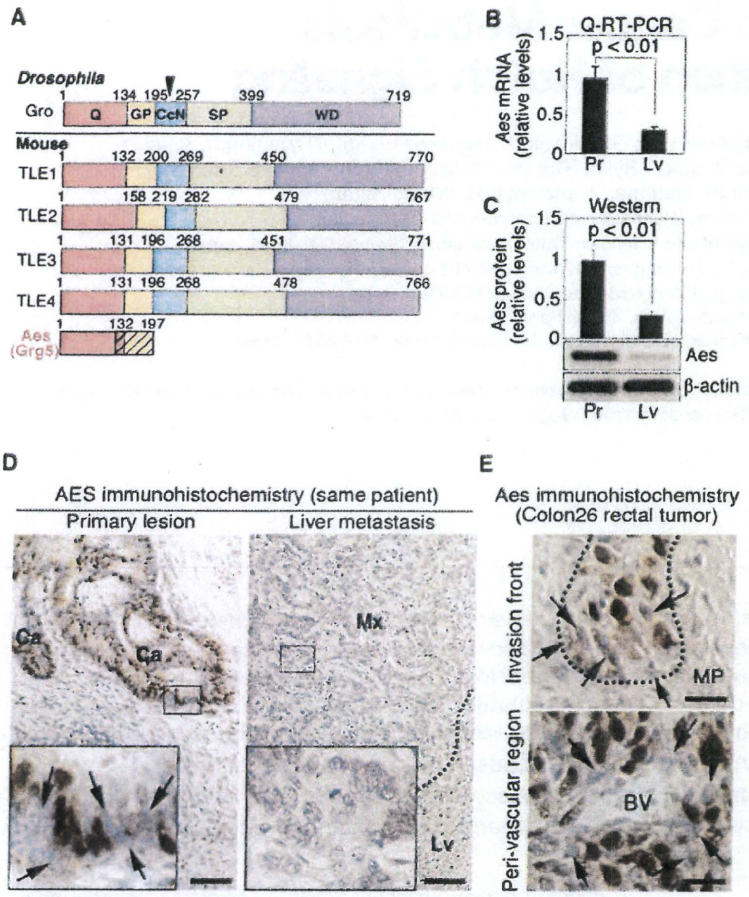

Figure 1. *Aes* as a Metastasis Suppressor Candidate

(A) Schematic representation of fly and mouse Gro/TLE family protein structures. Hatched region in Aes shows a limited identity with TLEs (~65%). Q, glutamine-rich domain (orange); GP, glycine-proline-rich domain (yellow); CcN, domain containing putative phosphorylation sites for cdc2 and casein kinase II (CK2) adjacent to nuclear localization signals (triangle) (blue); SP, serine-proline-rich domain (*green*); WD, domain containing series of tandem repeats of tryptophan and aspartic acid residues (purple). Numbers indicate amino acid residues.

(B) Expression levels of *Aes* mRNA in mouse Colon26 cells determined by quantitative (Q-)RT-PCR. Pr, primary tumors. Lv, liver metastases. Error bars indicate SD. (n = 3).

(C) Expression levels of Aes protein in Colon26 cells determined by western blotting. Same keys as in (B).

(D) Immunostaining for AES in a primary human colon cancer (left) and its liver metastasis (right) from the same patient. Boxed areas are shown in insets, respectively. Dotted line indicates the boundary between metastasis (Mx) and normal liver tissue (Lv). Note that some cancer cells at the invasive fronts had lost expression of *AES* (arrows). Ca, cancer epithelium. Scale bars, 100 μm. Nuclei were counterstained with hematoxylin.

(E) Loss of *Aes* expression on the invasive front of mouse Colon26 primary tumors (arrows). Dotted line indicates the boundary between invading cancer cells and host *muscularis propria* (MP). BV, blood vessel. Scale bars, 10 μm.

See also Figure S1.

1998). Even in such a model, the adenocarcinomas are only locally invasive, and neither intravasation nor distant metastasis is observed during the short life span of these mice. Accordingly, we have screened for candidate genes whose inactivation can stimulate metastasis of transplanted mouse colon cancer cells from the rectum to the liver, the commonest site of metastasis.

RESULTS

Aes as a Metastasis Suppressor Candidate

To identify genes responsible for metastasis suppression, we first prepared a syngeneic and orthotopic transplantation model of colon cancer metastasis in the mouse. When injected into the rectal smooth muscle layer, Colon26 cells can metastasize to the liver, lungs, and lymph nodes in the Balb/c hosts at different efficiencies (Corbett et al., 1975; Kashtan et al., 1992; Tsutsumi et al., 2001) (see Figures S1A–S1F available online). As a preliminary screening, we compared gene expression profiles between the primary tumors and their liver metastases using cDNA microarrays. While many genes showed differential expression, we focused on the category of "transcription regulator activity" in search for master regulators that control metastatic traits. Because cell migration and motility appear to be key traits of metastatic cancer (Christofori, 2006; Weinberg, 2007), we tested ~20 downregulated genes for inhibition of Colon26 invasion in vitro through Matrigel and found one that showed a strong activity, though it was at the 26th of the list (Figure S1G). This gene, *Amino-terminal enhancer of split* (*Aes*), also called *Grg5* in mice, is a member of the *Groucho/Transducin-Like Enhancer of split* (*Gro/TLE*) gene family, with its Q/GP domains showing similarities to those in TLEs (Gasperowicz and Otto, 2005; Lepourcelet and Shivdasani, 2002; Brantjes et al., 2001) (Figure 1A). Although mouse *Aes* helps development of bone and the pituitary gland (Mallo et al., 1995; Brinkmeier et al., 2003), its role in cancer progression has not been investigated. Consistent with the microarray and Matrigel results, mouse *Aes* was significantly downregulated in the liver and lung metastases, upon determinations by quantitative (Q-) RT-PCR (Figure 1B) and western blots (Figure 1C). Importantly, human liver metastatic lesions in 29 out of 52 colon cancer patients (i.e., 56%) expressed significantly lower levels of AES protein than primary tumors from the same patients (Figure 1D). Curiously, some cancer cells had already lost expression of *AES/Aes* at the invasion fronts in both human (Figure 1D, inset in the left panel) and mouse (Figure 1E) colon primary tumors. Furthermore, absence of AES in human colon cancer significantly correlated with vascular invasion ($p < 0.01$), distant metastasis ($p = 0.01$) and progression stages ($p = 0.02$; $n = 83$).

To investigate the roles of *Aes* in colon cancer metastasis, we constructed Colon26 cell derivatives whose *Aes* expression was

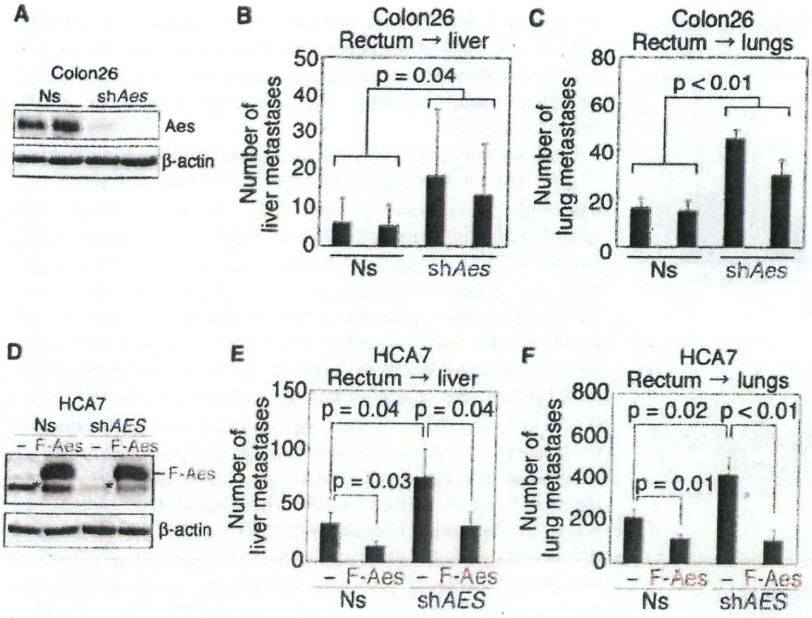

Figure 2. Suppression of Colon Cancer Metastasis by *Aes*

(A–C) Effects of *Aes* knockdown in mouse Colon26 cells (A) on their metastasis to the liver (B) and lungs (C), respectively. Multiple Colon26-derived clonal cell lines were isolated that expressed one of three different shRNA constructs, followed by the rectal transplantation. Data are shown for such cell lines derived from two distinct shRNA clones whose experiments were performed simultaneously, and similar data were obtained with a third clone (not shown). Ns, nonsilencing control. sh*Aes*, shRNA against *Aes* mRNA. Error bars indicate SD (n = 10).

(D–F) Effects of *Aes* overexpression in a human colon cancer cell line HCA7 (D) on its metastasis to nude mouse liver (E) and lungs (F) from the rectum, respectively. A clonal cell line expressing flag-tagged mouse Aes (F-Aes) was compared with a control containing the empty vector (–) (D); left half; Ns for nonsilencing control). The same set of cell lines were introduced with a construct that expressed an shRNA against human *AES* (sh*AES*; (D), right half). Asterisks show the band position for the endogenous human AES protein (western blot analysis). Note that metastasis-promoting effects of sh*AES* was suppressed by overexpression of mouse Aes (F-Aes), excluding the possibility of off-target effects by sh*AES*. Each data set shown is a representative of two. Error bars indicate SD (n = 5).

See also Figure S2.

knocked down constitutively by shRNA constructs (sh*Aes*) (Figure 2A). As anticipated, *Aes* knockdown promoted Colon26 metastasis from the Balb/c mouse rectum to liver (Figure 2B) and lungs (Figure 2C), for all clones derived from three independent shRNAs. Likewise, knockdown of human *AES* (Figure 2D) increased the number of metastases for HCA7 human colon cancer cells (Kirkland, 1985) to both liver (Figure 2E) and lungs (Figure 2F) of nude mice. Convincingly, this knockdown effect was reversed by overexpression of flag-tagged mouse *Aes* (F-Aes) that was not targeted by the shRNA against human *AES* (Figures 2D–2F). We then constitutively overexpressed *Aes* in Colon26 cells at the level five times higher than that of endogenous *Aes*, injected them into the mouse rectum, and found that their metastasis was suppressed significantly to both liver and lungs (Figures S2A–S2D). Notably, *Aes* suppressed lung metastasis of the cancer cells also upon intravenous injections (Figure S2E), another model of hematogenous metastasis that bypasses local invasion and intravasation (Price, 2001). Importantly, neither knockdown nor overexpression of *Aes* affected the size of primary tumors (Figures S2F–S2H). These results indicate that *Aes* suppresses colon cancer metastasis without affecting the growth of primary tumors.

Aes Is an Endogenous Notch Signaling Inhibitor

In colonic tumor formation and its malignant progression, Wnt, TGF-β, Hedgehog, and Notch signaling pathways appear to play key roles (Sancho et al., 2004; van Es et al., 2005; Taketo, 2006; Takaku et al., 1998), not to mention KRAS and p53. Interestingly, Gro/TLE cotranscription factors have been implicated in some of these pathways (Roose et al., 1998; Chen and Courey, 2000; Wang et al., 2002). We first investigated the possible role of Aes in Wnt signaling because of its Q and GP domains similar to those in TLE proteins that can inhibit the signaling (Brantjes et al., 2001). Although we confirmed repression by TLE1 to ~20%, Aes had only marginal effects on LEF1/β-catenin-induced TOPFLASH activation in HEK293 human embryonic kidney cells (Figure S3A). Aes also failed to suppress Wnt signaling in Colon26 cells (Figure S3B, left).

We then assessed the effects of Aes on other signaling pathways in colon cancer cells by transactivation assays using established luciferase reporters. Aes did not affect TGF-β or Hedgehog pathways (Figure S3B, center or right). Instead, Aes significantly inhibited Notch signaling, a critical signaling in development (Artavanis-Tsakonas et al., 1999; Huribut et al., 2007; Ilagan and Kopan, 2007), as determined by pGa981-6 reporter containing Rbpj (Recombination signal binding protein of the Jκ immunoglobulin gene, or CSL; CBF1 in human)-binding sites and a luciferase gene (Kato et al., 1997). Namely, expression of exogenously introduced *Aes* dose-dependently repressed both endogenous and RAMIC (Rbpj-associated molecule domain and intracellular domain of the Notch receptor, a recombinant protein equivalent to NICD, Notch intracellular domain) (Kato et al., 1997)-induced transcription of the reporter in Colon26 cells (Figure 3A). Of note, 293T cells showed the strongest activity of endogenous Notch signaling among 30 cell lines analyzed, and Aes caused tighter repression in these cells (to ~20%) (Figure S3C). Consistently, induction of Aes by doxycycline in Colon26 TetONF-Aes cells suppressed expression of endogenous Notch target *Hes1* (Figure S3D). On the other hand, knockdown of *Aes* doubled the activity of both the

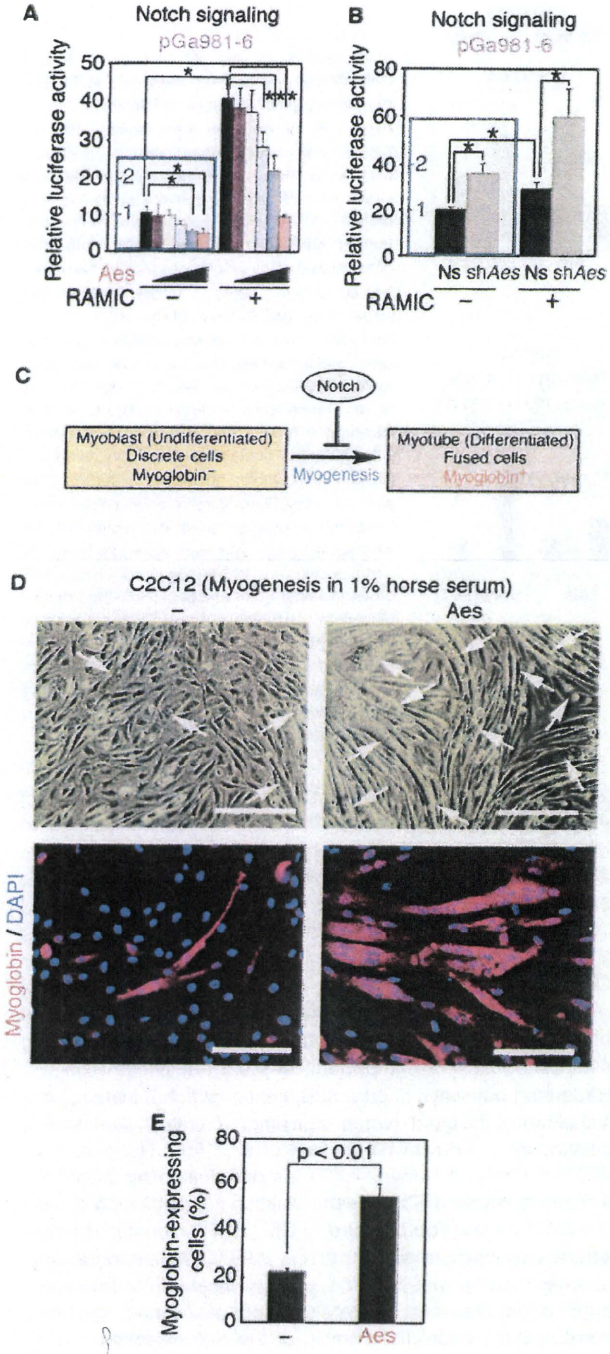

Figure 3. Inhibition of Notch Signaling by *Aes*

(A and B) Effects of *Aes* overexpression (A) and *Aes* knockdown (B) on Notch signaling in Colon26 cells determined by pGa981-6 luciferase reporter assay in the absence (–) or presence (+) of exogenously introduced RAMIC. Insets (blue frames) show the endogenous reporter activities. Ns, nonsilencing control. *$p < 0.01$ compared with the controls. Error bars indicate SD (n = 3).

(C) A schematic representation of the role of Notch signaling in myogenesis.

(D) Effects of Aes on myoblast differentiation. Rat C2C12 myoblasts were transfected with either the vector or Aes cDNA, and three stable clones were isolated, respectively. Myogenesis was induced by a medium containing 1% horse serum for 4 days. Myoglobin, a myotube marker, was immunostained (red) in C2C12 clones with or without overexpressed Aes. Nuclear DNA was stained with DAPI (blue). Arrows, myotubes with multiple nuclei. Scale bars, 100 μm.

(E) Quantification of the myoglobin-expressing cells in (D). Error bars indicate SD (n = 3).

See also Figure S3.

endogenous and RAMIC-induced Notch signaling in Colon26 cells (Figure 3B). Consistent with these data, *Aes* enhanced myogenic differentiation of C2C12 myoblasts in a representative biological assay for Notch signal inhibition (Kato et al., 1997) (Figures 3C–3E).

Because Aes and TLE proteins shared structural similarities (Figure 1A), we next asked whether TLE1 also inhibited Notch signaling. In contrast to Aes, TLE1 failed to repress the RAMIC-induced transactivation in 293T cells, human colon cancer HCT116 cells, and mouse Colon26 cells (Figure 4A; data not shown). Interestingly, however, coexpression with TLE1 significantly potentiated the repression by Aes. It was reported that Aes interacted with TLE1 in yeast (Pinto and Lobe, 1996), and we found coprecipitation of endogenous Aes and TLE1 in the lysates of colonic tumors from $Apc^{\Delta 716}$ mice (Oshima et al., 1995) (Figure 4B). Notably, we found nuclear colocalization of Aes and TLE1 forming distinct foci in $Apc^{\Delta 716}$ adenoma cells (Figure 4C). We further studied subcellular localization of Aes in cultured cells. When transfected alone, Aes fused to *Aequorea coerulescens* GFP (AcGFP-Aes) showed diffuse distribution in both the cytoplasm and nucleoplasm of live HCT116 cells (Figure 4D). Intriguingly, coexpression with TLE1 caused dramatic relocation of AcGFP-Aes to nuclei, causing distinct foci (Figure 4D). Similar results were obtained with 293T and Colon26 cells (data not shown).

We next employed deconvolution microscopy, and analyzed subnuclear localization of the Notch effectors; Rbpj, RAMIC (NICD), and Maml1 (Mastermind-like 1). In the absence of Aes/TLE1 complex, Rbpj, RAMIC, and Maml1 all showed diffuse nucleoplasmic distribution in HCT116 cells. When cotransfected with Aes and TLE1, however, RAMIC and Maml1 relocated to nuclear foci that also contained Aes and TLE1, whereas Rbpj distributed both in the foci and the nucleoplasm (Figures 4E and 4F).

To determine the roles of these nuclear foci in transcription, we performed in situ transcription labeling, and visualized BrUTP incorporation into mRNA during 5 min prior to fixation. When Notch effectors were coexpressed with Aes and TLE1, BrUTP uptake into mRNA was scarce in the nuclear foci where Maml1 resided (Figure 4G). These foci were not stained with anti-PML, anti-SC35, or anti-fibrillarin antibody, suggesting that they are distinct from PML bodies, RNA splicing bodies, and nucleoli (Zimber et al., 2004) (data not shown). Rather, lack of transcription in the foci was reminiscent of Bach2 foci, the nuclear bodies containing HDAC4 (Histone deacetylase 4) and SMRT (Silencing mediator of retinoid and thyroid receptor), and possibly related to matrix-associated deacetylase (MAD) bodies (Downes et al., 2000; Hoshino et al., 2007). In situ nuclear matrix preparation revealed that the Aes nuclear foci were indeed in the insoluble nuclear matrix fraction (Figure 4H). Moreover, HDAC3 was

associated and colocalized with Aes in the nuclear foci (Figure S4). Collectively, these results suggest that Aes, together with TLE1, can hold the Rbpj/NICD/Maml1 complex in nuclear foci where transcription is repressed.

Notch Signaling Inhibition Can Suppress Metastasis

Above results also suggested that *Aes* suppressed metastasis through inhibition of Notch signaling. As anticipated, attenuation of the signaling by constitutive expression of shRNA constructs against *RBPJ* mRNA (sh*RBPJ*) suppressed metastasis of HCA7 human colon cancer cells from the rectum to liver (multiplicity; 6.0 ± 2.7 versus 2.6 ± 1.6, $p = 0.02$) and to lungs (341 ± 89 versus 87 ± 40, $p < 0.01$) (Figures 5A and 5B) in nude mice. We obtained similar results also with mouse Colon26 cells expressing a dominant-negative mutant of Rbpj (dnRbpj; R218H; Kato et al., 1997) (Figures S5A and S5B). We then tested inhibition of Notch signaling with Compound E, a potent γ-secretase inhibitor (Milano et al., 2004; Schmidt, 2003; Zaczek et al., 1999) (GSI) (Figure 5C). It significantly suppressed metastasis of Colon26 cells to the liver (5.7 ± 5.5 versus 1.8 ± 2.4, $p = 0.04$) and lungs (54 ± 22 versus 18 ± 8, $p < 0.01$) (Figure 5D) from the rectum. Importantly, none of sh*RBPJ*, dnRbpj, or Compound E affected the size of primary tumors significantly (Figures S5C–S5E). Likewise, Compound E had little effect on the primary Colon26 tumors regarding their differentiation and proliferation (Figures S5F and S5G). These results underscore that Notch signaling plays an essential role in hematogenous metastasis of colon cancer cells.

Notch Activation by Stromal Ligands Induces Tumor Intravasation

Using immunofluorescence staining, we found that mouse Colon26 cells expressed abundant Notch1 receptor (Figure 6A, left), consistent with a report on human colon cancer (Zagouras et al., 1995). Notably, there was much Jagged1 ligand on the blood vessels in primary tumors (Figure 6A) as well as in their metastases to the liver (Figure 6B) and lungs (Figure 6C, left). Jagged1 was expressed also on normal epithelial cells in these organs (Figure 6B, Lv; hepatocytes: Figure 6C, right, Lg; pneumocytes expressing TTF-1). We also found that blood vessels and macrophages expressed another Notch ligand Delta-like 4 (Dll4) (Figures S6A–S6C). Curiously, activated NICD was detected in the tumor epithelium that was surrounded by DLL4-expressing stromal cells in human colon cancer tissues (Figure 6D). We employed the Q scoring (Detre et al., 1995), and obtained Spearman's correlation factor of 0.69, indicating a very strong association (0.6–0.8) between DLL4 and NICD expression ($p < 0.01$).

To test whether ligand-expressing stromal cells activated Notch signaling in cancer cells, we constructed "Notch reporter Colon26 ($C26^{RBS\text{-}EGFP}$) cells" that contained RBS (Rbpj binding sequence)-EGFP reporter, expressing EGFP upon Notch signal activation (Figure 6E). As expected, expression of RAMIC induced EGFP in the reporter cells in culture (Figure 6F). Convincingly, the EGFP staining was strongest in the $C26^{RBS\text{-}EGFP}$ cells located around blood vessels of the primary tumor in the Balb/c rectum (Figure 6G, left). Treatment of the tumor-bearing mice with Compound E, as well as overexpression of Aes in the reporter cells, almost eliminated expression of EGFP (Figure 6G, center and right), supporting that Aes acts through suppression of the Notch signaling. Interestingly, we found expression of EGFP in two types of metastasized cell clusters in the lung; micrometastases consisting of only a few cancer cells (Figure 6H, left), and cells at the periphery of larger metastases that were expanding in the lung parenchyma (Figure 6H, right) (see Discussion).

Because *Aes* was downregulated in cancer cells adjoining blood vessels (Figure 1E, bottom), we hypothesized that loss of *Aes* expression stimulated transendothelial migration (TEM) through Notch signal activation. To test the hypothesis in vitro, we placed cancer cells on a layer of HUVEC (human umbilical vein endothelial cells) that expressed Notch ligands (Lu et al., 2007; Mailhos et al., 2001). As expected, knocking down *Aes* in Colon26 cells stimulated HUVEC-induced Notch signaling as determined by Q-RT-PCR of *Hes1* mRNA (Figure 6I) and enhanced their TEM through the HUVEC layer (Figure 6J). Similar results were obtained with HCA7 cells (Figure S6D). Notably, expression of sh*RBPJ*s inhibited Notch signaling that was triggered by HUVEC (Figure 6K) and reduced their TEM significantly (Figure 6L). To observe TEM more dynamically, we took time-lapse movies of Colon26 cells with or without Aes induction migrating through the HUVEC cell layer (Movie S1). While approximately two-thirds of control Colon26 cells migrated underneath the HUVEC layer in 12 hr, only approximately one-third of the Aes-overexpressing Colon26 cells did (Figure S6E). We also found that recombinant DLL4 and JAGGED1 activated Notch signaling and enhanced motility of Colon26 cells when analyzed by simpler scratch assays (Figure S6F). These results are consistent with our hypothesis that *Aes* suppresses metastasis of colon cancer cells by inhibition of Notch signaling that stimulates cancer cell motility and TEM at the steps of local invasion, intravasation, and extravasation (see Discussion).

Aes Knockout Causes Tumor Intravasation

To test above hypothesis with endogenous tumors, we constructed a floxed allele of *Aes* (*Aes*^{f}), and introduced it into the $Apc^{\Delta 716}$ intestinal polyposis model carrying villin-Cre^{ERT2} transgene (*TgvCre*^{ERT2}) (el Marjou et al., 2004) whose tumors expressed substantial amounts of Aes (Figures 7A and 7B; Figures S7A and S7B). At 3 weeks of age, we treated the compound mutant $Apc^{+/\Delta 716}$-$Aes^{f/f}$-*TgvCre*^{ERT2} with 4-hydroxytamoxifen (4HT) to activate Cre recombinase in the intestinal epithelium, generating $Apc^{+/\Delta 716}$-$Aes^{\Delta ex2/\Delta ex2}$-*TgvCre*^{ERT2} genotype (*Apc/Aes*). In these mice that had lost *Aes* exon 2 (Figure S7C), we found marked tumor invasion and intravasation into the smooth muscle layer of the small intestine and colon (Figures 7D and 7E; *Apc/Aes*). Although all *Apc/Aes* mutants (25 examined) showed this invasion phenotype at 17 weeks of age, $Apc^{\Delta 716}$ polyposis mice never did (Kitamura et al., 2007; Oshima et al., 1995; Takaku et al., 1998) (Figure 7C; *Apc*). For the *Apc/Aes* polyps larger than 2 mm in diameter, about half of them was found invading into the submucosa or beyond (Figure 7F).

Strikingly, many of the invading tumor glands in the *Apc/Aes* mice were found inside vessels that were often distended, reminiscent of tumor embolism (Figure 7G, left). This intravasation was further confirmed by immunofluorescence for epithelial marker cytokeratin and vessel marker CD31 or blood vessel marker VE-cadherin (Figure 7G, center and right, respectively). Although such intravasating tumor epithelial cells should be

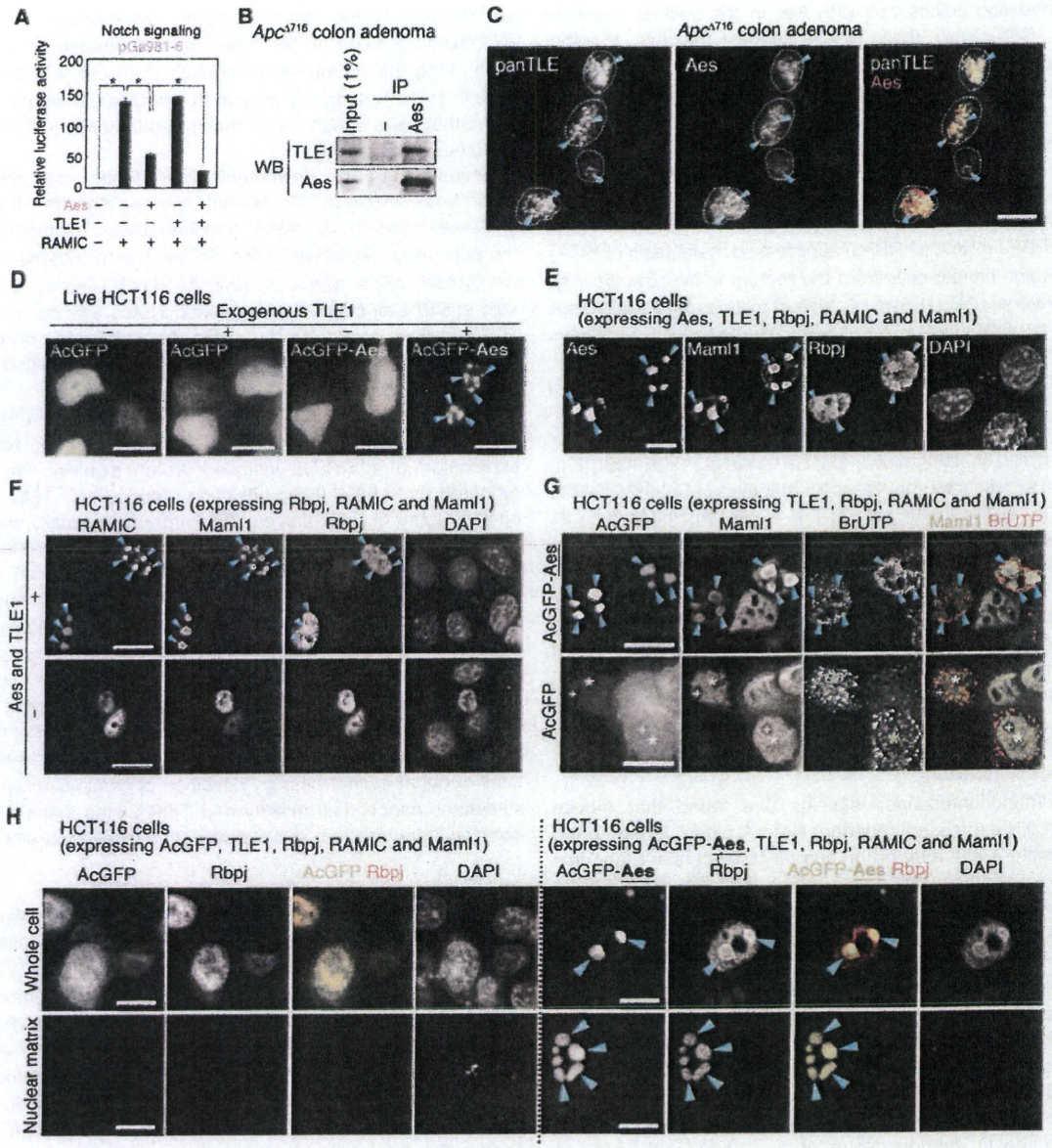

Figure 4. Colocalization of Aes and TLE1 with Notch Pathway Proteins in Nuclear Foci

(A) Effects of overexpression of Aes and TLE1 on RAMIC-induced Notch signaling determined by pGa981-6 luciferase reporter in HEK293 cells. *$p < 0.01$. Error bars indicate SD ($n = 3$).

(B) In vivo interaction between endogenous Aes and TLE1 in colonic adenomas of $Apc^{\Delta 716}$ mice. Aes in the tumor lysates was immunoprecipitated (IP) using anti-Aes antibody. Subsequently, Aes and TLE1 in the precipitates were detected by western blotting (WB).

(C) Immunofluorescence of endogenous TLE and Aes in an $Apc^{\Delta 716}$ colon adenoma. TLE proteins were detected by anti-panTLE antibody that had been raised against WD repeats. Arrowheads indicate colocalization of TLE and Aes in the nucleus (circled by broken lines). Scale bar, 10 μm.

(D) Effects of TLE1 overexpression on localization of Aes. HCT116 cells were transfected with expression plasmids for AcGFP or AcGFP-Aes simultaneously with or without TLE1. Twenty-four hours after transfection, localization of AcGFP in live cells was analyzed under a fluorescent microscope. Scale bars, 10 μm.

(E) Immunofluorescence of overexpressed Aes, Maml1, and Rbpj in HCT116 cells. Note colocalization of Aes, Maml1, and Rbpj in nuclear foci (arrowheads). Scale bar, 10 μm.

(F) Immunofluorescence of overexpressed RAMIC, Maml1 and Rbpj in HCT116 cells. Note colocalization of Maml1, RAMIC, and Rbpj in nuclear foci in the presence of Aes and TLE1 (arrowheads). Scale bars, 10 μm.

(G) Effects of Aes and TLE1 on localization of Maml1 and transcription activity in the nucleus. HCT116 cells were transfected with expression plasmids for TLE1, Maml1, RAMIC and simultaneously with or without AcGFP-Aes and TLE1. Twenty-four hours later, the transfectants were pulse-labeled with BrUTP. Anti-BrUTP antibody localized newly synthesized mRNA in the nucleus. Note that Aes and Maml1 colocalized in the nuclear foci where few BrUTP speckles were observed

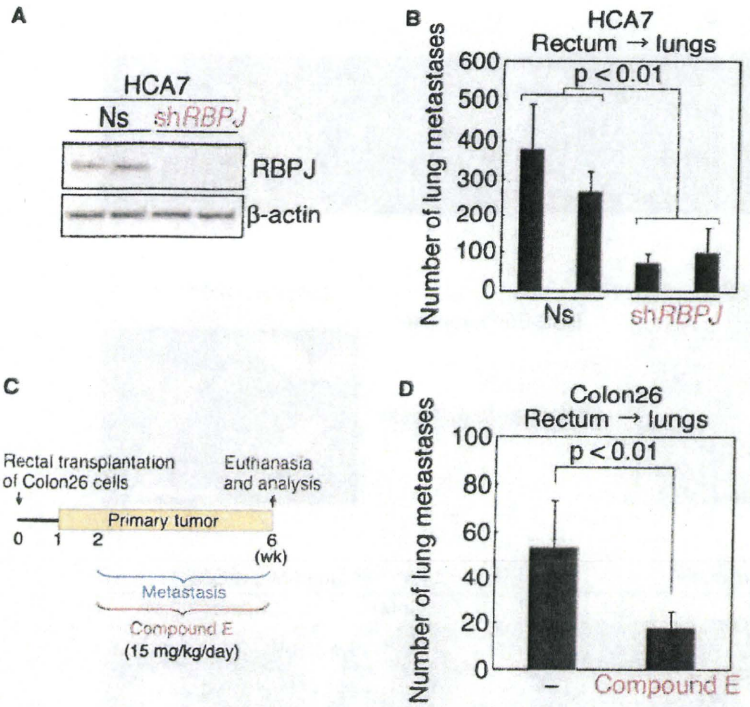

Figure 5. Suppression of Colon Cancer Metastasis by Inhibition of Notch Signaling

(A) Construction of HCA7 derivatives with constitutive expression of shRNA sequences against *RBPJ* mRNA (sh*RBPJ*), confirmed by western blotting. Clones were isolated using two different shRNAs. β-Actin is shown as a loading control. Ns, nonsilencing controls.

(B) Effects of sh*RBPJ* on lung metastasis of HCA7 derivatives transplanted into the nude mouse rectum. Error bars indicate SD (n = 10).

(C) Dosing scheme of Compound E for mice bearing Colon26 rectal tumors.

(D) Effects of Compound E on lung metastasis of Colon26 rectal tumors in Balb/c mice. –, Vehicle control. Data set shown is a representative of two. Error bars indicate SD (n = 8).

See also Figure S5.

called "adenocarcinomas" by histopathological definition, the extent of cellular atypia and epithelial architecture were rather similar to those in the $Apc^{\Delta 716}$ adenomas, without a very malignant appearance.

As in the transplantation results above (Figures S6A–S6C), blood vessels and macrophages expressed Dll4 ligand also in the *Apc/Aes* tumors (Figures 7H–7K). In addition, we found that smooth muscle layers as well as *muscularis mucosae* also expressed Dll4 ligand, although the invading tumor epithelium scarcely did (Figures 7L and 7M). Notably, the expression level of tumor *Hes1* was 1.5 times higher in *Apc/Aes* compound mutants than in *Apc* mutants (Figure 7N). Furthermore, treatment of the *Apc/Aes* mice with Compound E inhibited the tumor invasion significantly (Figure 7O), indicating a key role of Notch signaling in the invasion that was caused by *Aes* knockout. On the other hand, knocking out *Aes* did not affect the tumor size or number (Figure 7P).

DISCUSSION

In this study, we have demonstrated that *Aes* inhibits metastasis of colon cancer cells in an orthotopic transplantation model in mice. With conditional *Aes* knockout mutation in $Apc^{\Delta 716}$ polyposis mice, intestinal tumors showed local invasion and intravasation, two earliest steps in the metastatic cascade. These results indicate that inactivation of *Aes* accelerates local invasion and intra/extravasation, and plays critical roles in the metastatic spread of endogenous tumors. The invasion histopathology of the *Apc/Aes* mutants was distinctly different from that of the *cis-Apc/Smad4* adenocarcinomas. The latter tumors were surrounded by immature myeloid cells (iMCs; $CD34^+CD45^+CCR1^+$) and showed local invasion without intravasation (Kitamura et al., 2007; Kitamura and Taketo, 2007). In contrast, there were few iMCs around the invasion fronts of *Apc/Aes* tumors (data not shown), suggesting that tumors of these two models invade by different mechanisms.

Proliferation of Colon26 cells remained unaffected by *Aes* overexpression or knockdown, either in culture or upon grafting to the mouse rectum (Figures S2F–S2H; data not shown). Furthermore, the tumor number or size was not affected by the conditional *Aes* knockout (Figure 7P). Therefore, we conclude that *Aes* is an endogenous "metastasis suppressor" that inhibits metastasis but not tumorigenicity (Steeg, 2006; Smith and Theodorescu, 2009).

During the short life span of the *Apc/Aes* mutant mice (<18 weeks), we have been unable to find any overt metastasis in either liver or lungs. Because we initially used Colon26 cell line to find *Aes* gene downregulation in liver metastasis, we reasoned this difference from the *Apc/Aes* phenotype as below. First, the method of Colon26 injection into the rectal smooth muscle bypasses the local invasion, as well as intravasation

(arrowheads). On the other hand, in the absence of Aes, Maml1 distributed throughout the nucleoplasm where BrUTP was present (asterisks). Different from the top row photo, BrUTP-unstained area in AcGFP (bottom; marked as +) are also unstained for Maml1 in the left panel, suggesting that these areas are nucleoli rather than the foci. Scale bars, 10 μm.

(H) Colocalization of Aes and Rbpj on the nuclear matrix. HCT116 cells were transfected with expression plasmids for AcGFP or AcGFP-Aes simultaneously with TLE1, Rbpj, RAMIC, and Maml1. Twenty-four hours later, localization of the overexpressed proteins was analyzed by immunofluorescence (arrowheads in Whole cell). Note that AcGFP-Aes and Rbpj were retained inside the cells even after soluble proteins were washed off (arrowheads in Nuclear matrix). In contrast, Rbpj did not remain in the cells in the absence of Aes. Scale bars, 10 μm.

See also Figure S4.

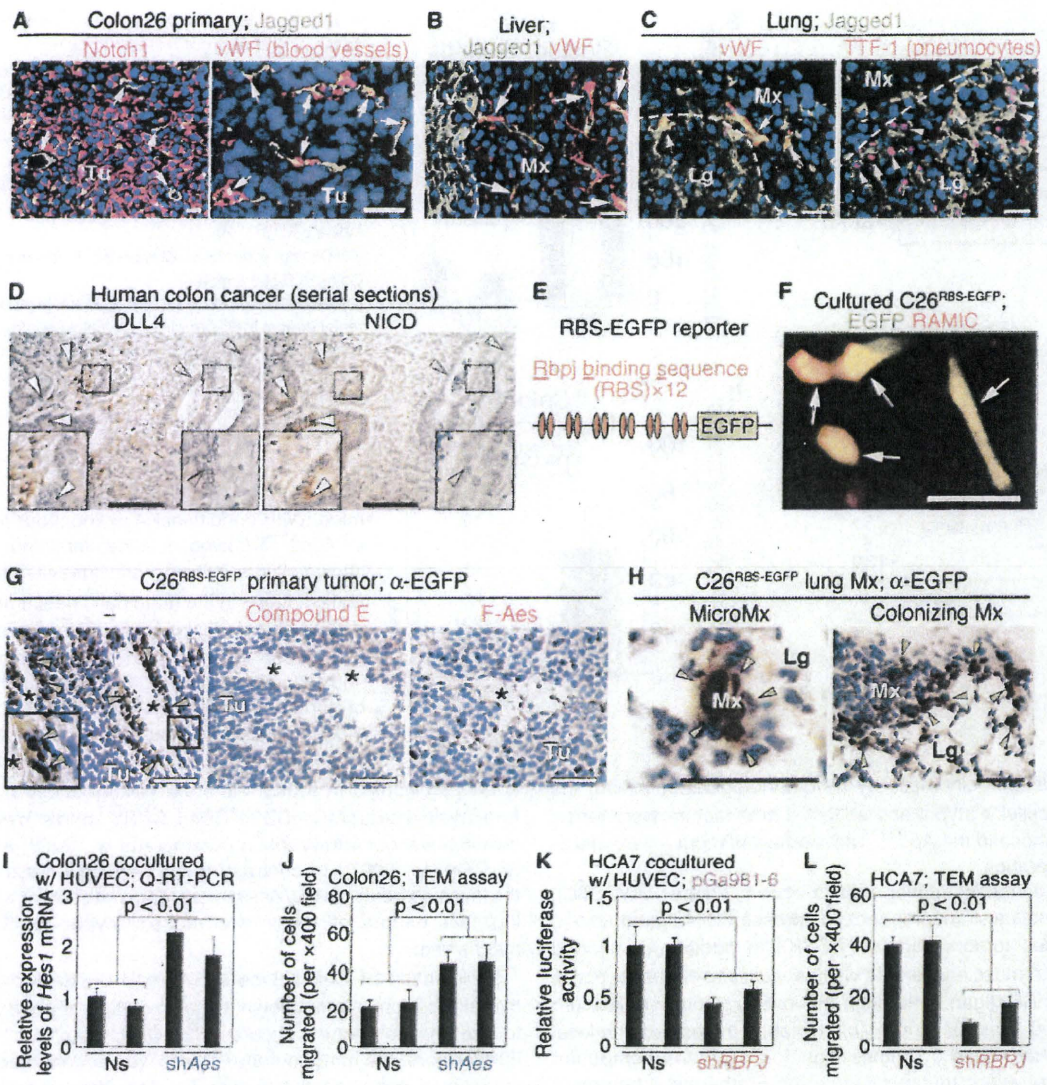

Figure 6. Activation of Notch Signaling in Cancer Cells by Adjoining Blood Endothelial Cells and Macrophages

(A) Immunofluorescence staining of Jagged1 (green) in a Colon26 tumor of the rectum. Red staining shows Notch1 (left) or blood vessel marker vWF (von Willebrand factor; right). DNA was stained with DAPI (blue). Arrows point representative Jagged1-expressing blood vessels. Tu, Tumor. Scale bars, 10 μm.

(B and C) Immunofluorescence staining of Jagged1 (green) in the liver (B) and lung (C) with Colon26 metastases. Red staining shows vWF, or Thyroid transcription factor (TTF) −1, a pneumocyte marker (C; right). Arrows and arrowheads point to the representative Jagged1-expressing blood vessels and pneumocytes adjoining the metastatic foci, respectively. Broken lines indicate the boundaries between the metastases and liver or lung tissues. Mx, metastasis. Lv and Lg, normal liver and lung tissues, respectively. DNA was stained with DAPI (blue). Scale bars, 10 μm.

(D) Close proximity of DLL4-expressing cells with NICD-expressing cells in human colon cancer. Serial sections were immunostained with anti-DLL4 (left) and anti-NICD (right) antibodies, respectively. Note that DLL4 was expressed in the stroma close to the cancer epithelium where NICD was stained (closed arrowheads in left insets). In contrast, cancer epithelium surrounded by DLL4-negative stroma showed little NICD staining (open arrowheads in right insets). Bars, 100 μm.

(E) A schematic representation of the RBS-EGFP reporter construct. The Notch signaling causes expression of EGFP through the tandem repeats of Rbpj binding sequence (RBS). The reporter was introduced into Colon26 cells to derive $C26^{RBS\text{-}EGFP}$ cells.

(F) Induction of EGFP in response to RAMIC expression in $C26^{RBS\text{-}EGFP}$ cells. An expression vector for myc-tagged RAMIC was transfected into the $C26^{RBS\text{-}EGFP}$ cells. Autofluorescence of EGFP and immunofluorescence signal of myc (red) were photographed under a fluorescence microscope, and merged electronically. Note that EGFP was induced in most of the RAMIC-expressing cells, merging as yellow (arrows). Scale bar, 10 μm.

(G and H) Activation of the Notch signaling within Colon26 primary tumors of the rectum (G, left) and its metastasis to the lung (H), detected by immunostaining for EGFP (green arrowheads). Boxed area in the left panel of (G) is enlarged in the inset. Note that treatment with Compound E (G, center) or overexpression of flag-tagged Aes (G, right) suppressed induction of EGFP. Asterisks, blood vessel lumens. Tu, tumor. Mx, metastasis. Lg, normal lung tissue. Scale bars, 50 μm.

because some fine vessels are destroyed upon injection. Second, Colon26 cells contain an activated *Kras* mutation allele. Accordingly, additional mutations in the *Apc/Aes* mutant mice may lead to overt metastasis of the intestinal tumors to distant organs.

Curiously, some of the cancer cells had already lost expression of *AES/Aes* on the invasion fronts in both human (Figure 1D, inset in the left panel) and mouse (Figure 1E) colon primary tumors. These results suggest that expression of *AES/Aes* is downregulated during the expansion of primary tumors. When cancer cells lose Aes, they can acquire the capacity to invade and intravasate. The mechanisms by which expression of Aes is downregulated remain to be investigated. We searched for *AES* mutations in colon cancer cell lines, without evidence so far. Although we tested the possibility of DNA methylation by treating colon cancer cell lines that lack AES with 5-aza-2-deoxycytidine, we found no increases in its expression. Thus, we speculate that *AES/Aes* gene is inactivated through some epigenetic changes other than DNA methylation.

Interestingly, we found that Aes colocalized with TLE1, Rbpj, RAMIC and Maml1 in nuclear foci where transcription is repressed (Figures 4D–4H). Because Aes is also associated and colocalized with HDAC3 in the foci (Figure S4), we speculate that Aes converts the transactivation complex to the MAD (matrix-associated deacetylase) bodies where HDAC proteins repress the Rbpj-dependent transcription (Kao et al., 1998; Downes et al., 2000). These results are consistent with reports that Notch repressors including SMRT and Mint/Sharp/Spen also show a similar speckled pattern in the nucleus (Kao et al., 1998; Downes et al., 2000; Oswald et al., 2002; Shi et al., 2001). Curiously, *Aes* null mice show a dwarf phenotype (Mallo et al., 1995, and data not shown). The dwarfism is caused by reduction in growth hormone-producing cells in the pituitary (Brinkmeier et al., 2003). Notably, the same dwarf phenotype is also reported in the transgenic mice overexpressing NICD, and in conditional knockout mice of the *Mint* gene (Zhu et al., 2006; Yabe et al., 2007), supporting the Notch-suppressing role of Aes in vivo.

It is possible that the elementary processes stimulated by Notch signaling are the motility and migration as implicated by our initial analysis of Aes in Matrigel (Figure S1G) and simpler scratch assays using recombinant Notch ligands (Figure S6F). Thus, we speculate that the enhanced motility contributes to TEM activity of cancer cells. It is conceivable that Notch signaling affects, either directly or indirectly, a series of small G proteins of the Rho family that can control the assembly of the actin cytoskeleton, as cell motility is regulated by such molecules (Weinberg, 2007). While these steps may be achieved by some carcinoma cells through a program of epithelial-mesenchymal transition (EMT), we have been unable to find signs of EMT in the Notch signaling-activated colon cancer or intestinal tumor cells. For example, tumor cells in the *Apc/Aes* compound mutants retained expression of cytokeratins and E-cadherin (Figures 7G–7I; data not shown) whose loss is a hallmark of EMT (Weinberg, 2007). Furthermore, expression of *Snail*, *Slug*, or *Twist* in Colon26 cells did not change upon transfection of *Aes* (data not shown). So far, about ten metastasis suppressor genes have been reported (Steeg, 2006; Smith and Theodorescu, 2009). Many of them appear to be involved in later steps in the metastasis cascade such as colonization, whereas some are involved in signal transduction pathways, including MAP kinase, Rho, Rac, and G protein-coupled and tyrosine kinase receptors. The effects of Aes downregulation in mutant mice on these genes remain to be investigated.

We found that Notch ligands Jagged1 and Dll4 were present on endothelial cells of the liver and lungs. Furthermore, we found ligand expression also on normal epithelium of the metastasis target organs (Figures 6B and 6C; Figures S6B and S6C). Convincingly, we found activated Notch signaling (expression of EGFP as a readout) in two types of metastasized cell clusters in the lung; micrometastases consisting of only a few cancer cells, and cells at the periphery of larger metastases that were expanding in the lung parenchyma (Figure 6H). Considering the fact that Aes can inhibit metastasis of cancer cells injected intravenously, we speculate that Aes also attenuates extravasation at the target organs. In addition, the ligand-expressing parenchymal cells adjoining the cancer cells may facilitate the metastatic expansion through stimulation of cancer invasion into the surrounding tissues, and inhibition of apoptosis in cancer cells (Artavanis-Tsakonas et al., 1999).

By searching the ONCOMINE database (http://www.oncomine.org/), we found that data were compiled showing the correlation between *AES* downregulation and metastasis for a variety of cancers such as prostate, bladder, breast, and ovarian cancers, and sarcoma, neuroblastoma, etc. These data suggest that *AES* has a metastasis-suppressing role also in other types of cancer. Furthermore, these results imply that earlier steps of the invasion-metastasis cascade are probably similar in various types of human tumors, although the last step—colonization—is likely to depend on complex interactions between the metastasizing cells and microenvironments of the host tissues where they land (Weinberg, 2007).

In summary, we have demonstrated that *Aes* is a metastasis suppressor that prevents local tumor invasion and intravasation through inhibition of Notch signaling. When cancer cells retain expression of *Aes*, it suppresses Notch signaling that is triggered

(I) Effects of *Aes* knockdown by shRNA against *Aes* mRNA (sh*Aes*) on Notch signaling. Colon26 cells with (sh*Aes*) or without (Ns; nonsilencing) constitutive expression of sh*Aes* were cocultured with HUVEC. Twelve hours later, cells were harvested and expression of mouse *Hes1* mRNA was quantified. Error bars indicate SD (n = 3).

(J) Effects of sh*Aes* on transendothelial migration (TEM) of Colon26 cells. Twenty-four hours after coculture, Colon26 cells that had migrated through the HUVEC layer were counted. Error bars indicate SD (n = 3).

(K) Effects of shRNA against *RBPJ* mRNA (sh*RBPJ*) on Notch signaling. Two independent HCA7 clones were derived by introducing nonsilencing control (Ns) and *RBPJ* knockdown (sh*RBPJ*) constructs, respectively, and transfected with the luciferase reporter followed by coculture with HUVEC. At 12 hr posttransfection, luciferase activity was determined. Error bars indicate SD (n = 3).

(L) Effects of sh*RBPJ* on TEM activity of HCA7 cancer cells. HCA7 cells were placed on a layer of HUVEC. Twenty-four hours later, HCA7 cells were counted that had migrated through the HUVEC layer. Error bars in (I–L) indicate SD of three independent experiments.

See also Figure S6 and Movie S1.

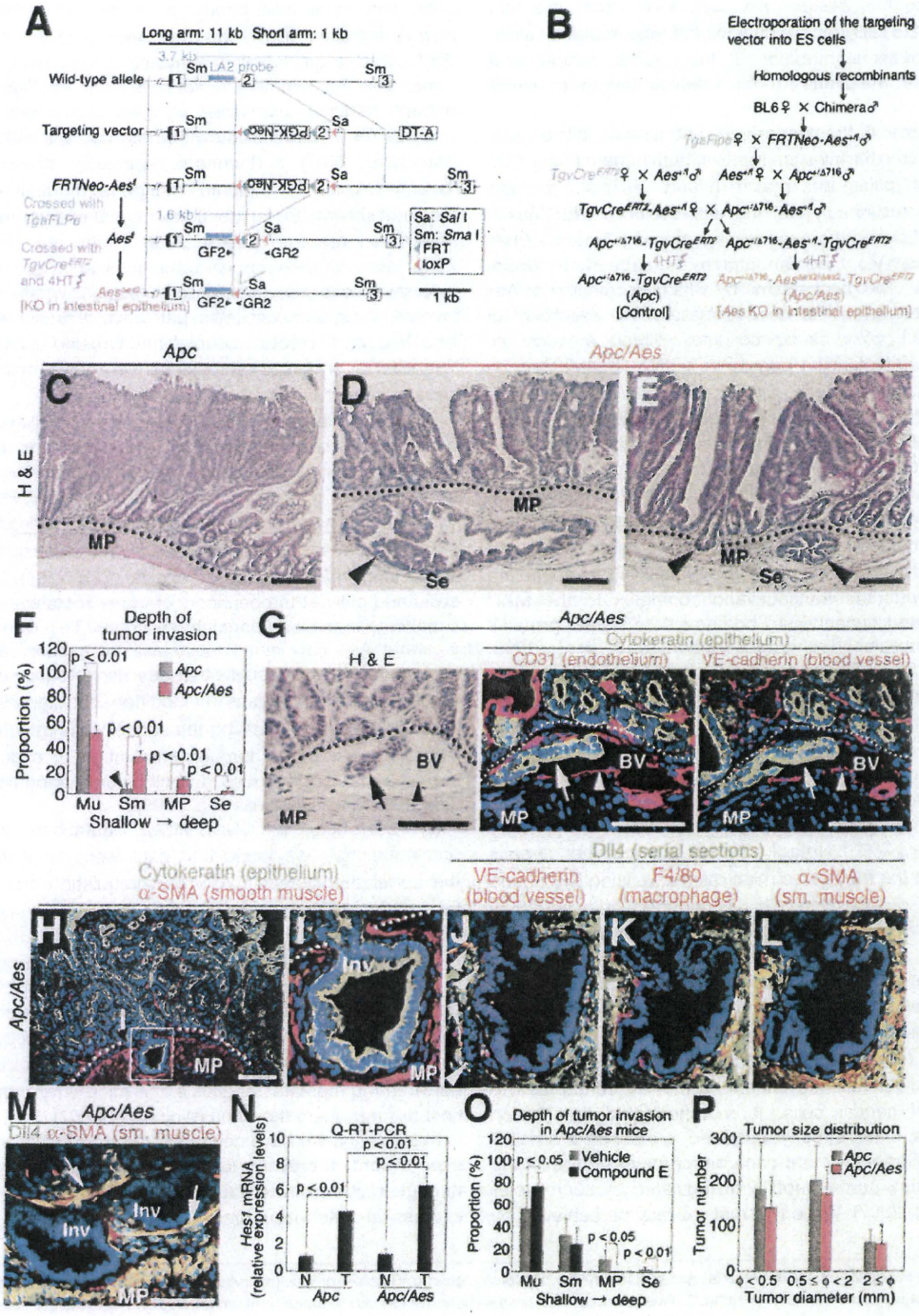

Figure 7. Local Tumor Invasion and Intravasation Phenotypes of the Compound Knockout Mice for *Aes* and *Apc* Genes

(A) Targeting strategy for the *Aes* allele specifically in the intestinal epithelium. Restriction sites and a Southern blotting probe are shown. PCR primers GF2 and GR2 were used to distinguish the floxed allele (Aes^{f}) from the targeted allele ($Aes^{\Delta ex2}$) of *Aes* gene after Cre activation by 4-hydroxytamoxifen (4HT).

(B) Breeding scheme for generating $Apc^{+/\Delta 716}$-$Aes^{f/f}$-$TgvCre^{ERT2}$ compound mutants. Germline mice with the targeted *Aes* allele flanked by a PGK-Neo cassette ($FRTNeo\text{-}Aes^{+/f}$) were crossed with a transgenic strain where expression of Flpe was driven by actin promoter (*TgaFlpe*) to remove the cassette. Resulting $Aes^{+/f}$ mice were crossed with another transgenic strain carrying an expression cassette for Cre^{ERT2} driven by villin promoter ($TgvCre^{ERT2}$) and *Apc* knockout mice ($Apc^{+/\Delta 716}$), to generate $Apc^{+/\Delta 716}$-$Aes^{f/f}$-$TgvCre^{ERT2}$ compound mutant mice. Treating them with 4HT activated Cre^{ERT2}, knocking out the *Aes* gene (*Apc/Aes*).

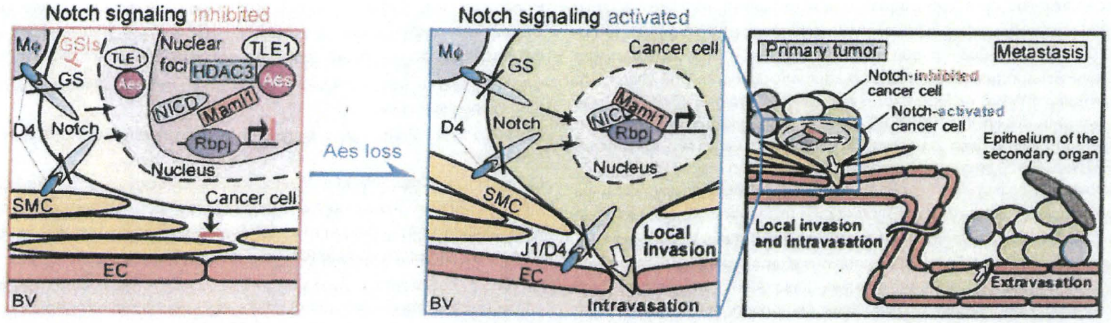

Figure 8. A Schematic Representation of *Aes* as a Notch Signaling Inhibitor, Hence a Metastasis Suppressor

When Notch receptor on a cancer cell is bound by Dll4 (D4) or Jagged1 (J1) ligand on adjoining macrophages (Mϕ), smooth muscle cells (SMC), or endothelial cells (EC), Notch intracellular domain (NICD) is released by γ-secretase (GS) cleavage. We propose that Aes relocates to nuclear foci with TLE1, Rbpj, NICD, Maml1, and HDAC3, to repress transcription (left). Once Aes is lost in a cancer cell, the transcription is derepressed, stimulating its local invasion and intravasation into the blood vessel (BV, center). In addition, Notch signaling is likely to promote extravasation of the cancer cell at the target organ, enhancing its metastasis (right). GSIs, GS inhibitors.

by the stromal cells (Figure 8, left). Once cancer cells lose its expression, derepressed Notch signaling can stimulate their local invasion (Figure 8, center), enhancing intravasation to promote metastasis (Figure 8, right). Because numerous compounds and biologicals have been evaluated as Notch signaling inhibitors, it is possible that some of such agents prove clinically efficacious in the treatment and prevention of cancer metastasis.

EXPERIMENTAL PROCEDURES

Animals

Balb/c, C57BL/6, and nude mice were purchased from CLEA (Japan). *Apc*$^{\Delta 716}$ and *TgvCre*^{ERT2} mice have been described previously (Oshima et al., 1995; el Marjou et al., 2004). *TgaFlpe* mice were obtained from the Jackson Laboratory. All animal experiments were conducted according to the protocol approved by the Animal Care and Use Committee of Kyoto University.

Microarray Analysis

RNA samples were prepared from Colon26 cells in primary tumors and their liver metastases using TRI reagent (SIGMA). Gene expression profiles were analyzed using 3D-Gene Mouse Oligo Chip 24k (TORAY).

Clinical Samples

Cancer tissues had been resected from patients who had undergone operations with informed consents, with the protocol approved by the Ethics Committee of Kyoto University or Kitano Hospital. Tumors were fixed by formalin and embedded in paraffin wax.

Conditional Knockout of *Aes* Allele

As shown in Figure 7A, we constructed a targeting vector where the PGK-Neo cassette sandwiched with FRT sequences was inserted into intron 1 immediately 5′ to exon 2 of *Aes*, followed by addition of loxP sequences sandwiching the insert and exon 2. The vector was constructed using the recombineering technology (Liu et al., 2003). A BAC clone bMQ-222K13 containing whole *Aes* gene of 129 strain was obtained from Geneservice (UK). A 13 kb DNA fragment spanning from 8 kb upstream of exon 1 to 2 kb downstream of exon 2 was retrieved from the BAC, and subcloned into pMCS-DTA vector to construct "pMCS-DTA-Aes" using SW102 strain of *Escherichia coli*. A PGK-Neo cassette sandwiched with two loxP sequences was excised from PL452 plasmid and inserted at downstream of exon 2 in pMCS-DTA-Aes to construct "pMCS-DTA-loxNeo-Aes." After induction of Cre recombinase by arabinose in SW106 strain of *E.coli*, the pMCS-DTA-loxNeo-Aes was introduced into the SW106. Upon Cre-mediated excision of the PGK-Neo cassette, one loxP sequence was left at downstream of exon 2, creating "pMCS-DTA-lox-Aes." Then a PGK-Neo cassette sandwiched with two FRT

(C–E) Histopathology of the small intestine at 17 weeks of age (H & E). In the control (*Apc*), adenoma cells remained above the *muscularis mucosae* (dotted line; C). In the *Apc/Aes* compound mutant mice, tumor cells invaded the *muscularis mucosae* and *muscularis propria* (MP), reaching the *serosa* (Se) (arrowheads in D and E). Scale bars, 100 μm.

(F) Quantification of the depth of tumor invasion in the small intestine at 17 weeks of age. Note that the tumor cells in the compound mutants (*Apc/Aes*; red) but not controls (*Apc*; gray) deeply invaded into the *submucosa* (Sm). Mu, *mucosa*. MP, *muscularis propria*. Se, *serosa*. Arrowhead, pseudoinvasion (herniation) in *Apc* control. n = 5 for each group.

(G) Tumor intravasation in the *Apc/Aes* mice. Left, An H&E staining suggested tumor cells (arrow) inside a blood vessel (BV; also indicated by arrowhead) near the *muscularis mucosae* (dotted line). This interpretation was verified by immunofluorescence in the adjoining sections for epithelial marker cytokeratin (green; arrow), and vessel marker CD31 (red; center) as well as blood vessel marker VE-cadherin (right). MP, *muscularis propria*. Scale bars, 50 μm.

(H–L) Expression of Dll4 ligand on stromal cells analyzed by immunostaining of serial sections. Epithelial cells express cytokeratin (green), whereas smooth muscle cells (MP; *muscularis propria*) express α-smooth muscle actin (α-SMA in red; H). Boxed area in (H) is enlarged in (I), whose serial sections are (J), (K), and (L). Blood vessels (stained for VE-cadherin in red; J), macrophages (F4/80 in red; K), and smooth muscle (α-SMA in red; L) expressed Dll4 (green) merging as yellow (arrowheads) around the local invasion of tumor epithelium. Scale bar, 100 μm.

(M) Immunofluorescence of Dll4 (green) and α-SMA (red) in the invading tumor of the *Apc/Aes* mutant (Inv). Note that smooth muscle cells in the *muscularis mucosae* (arrows) as well as the *muscularis propria* (MP) expressed Dll4 ligand. Scale bar, 50 μm.

(N) Expression levels of *Hes1* mRNA in the mouse small intestine determined by Q-RT-PCR. N, normal mucosa. T, tumor. Error bars indicate SD (n = 5).

(O) Effects of Compound E on depth of tumor invasion. *Apc/Aes* mice were treated with (black bars) or without (gray bars) Compound E for 10 weeks. Error bars indicate SD (n = 5 for each group).

(P) Size distribution of tumors in the small intestine at 17 weeks of age. Control *Apc* is shown in gray, whereas *Apc/Aes* is indicated in red. Error bars indicate SD (n = 5).

See also Figure S7.